×

Charge-Separation in Panchromatic, Vertically Positioned Bis(donorstyryl)BODIPY – Aluminum(III) Porphyrin – Fullerene Supramolecular Triads

Journal:	*Nanoscale*
Manuscript ID	NR-ART-08-2018-006649.R1
Article Type:	Paper
Date Submitted by the Author:	24-Sep-2018
Complete List of Authors:	Zarrabi, Niloofar; University of Minnesota Duluth Obondi, Chris; University of North Texas, Department of Chemistry Lim, Gary; UNT, Chemistry Seetharaman, Sairaman; University of North Texas Boe, Benjamin; University of Minnesota Duluth DSouza, Francis; University of North Texas, Department of Chemistry Poddutoori, Prashanth; University of Minnesota Duluth, Chemistry&Biochemistry

×

ROYAL SOCIETY OF CHEMISTRY

Nanoscale

ARTICLE

Charge-Separation in Panchromatic, Vertically Positioned Bis(donorstyryl)BODIPY – Aluminum(III) Porphyrin – Fullerene Supramolecular Triads

Niloofar Zarrabi,[a] Christopher O. Obondi,[b] Gary N. Lim,[b] Sairaman Seetharaman,[b] Benjamin G. Boe,[a] Francis D'Souza,*[b] Prashanth K. Poddutoori*[a]

Three, broad band capturing, vertically aligned supramolecular triads, R_2-BDP-AlPorF$_3$←Im-C$_{60}$ [R = H, styryl (C$_2$H$_2$-Ph), C$_2$H$_2$-TPA (TPA = triphenylamine); ← = coordinate bond], are constructed using BODIPY derivative (BDP, BDP-Ph$_2$ or BDP-TPA$_2$), 5,10,15,20-tetrakis(3,4,5-trifluorophenyl)aluminum(III) porphyrin (AlPorF$_3$) and fullerene (C$_{60}$) entities. The C$_{60}$ and BDP units are bound to the Al center on opposite faces of the porphyrin; the BDP derivative through a covalent axial bond using a benzoate spacer, and the C$_{60}$ through a coordination bond via an appended imidazole. Owing to the bisstyryl functionality on BDP, the constructed dyads and triads exhibited panchromatic light capture. Due to the diverse absorption and redox properties of the selected entities, it was possible to demonstrated excitation wavelength dependent photochemical events. In the case of BDP-AlPorF$_3$ dyad, selective excitation of BDP resulted in singlet-singlet energy transfer to AlPorF$_3$ (k_{EnT} = 1.0 x 10^{10} s^{-1}). On the other hand, excitation of AlPorF$_3$ entity in BDP-AlPorF$_3$←Im-C$_{60}$ triad, revealed charge separation leading to BDP-(AlPorF$_3$)$^{+•}$–(C$_{60}$)$^{-•}$ charge separated state (k_{CS} = 2.43 x 10^9 s^{-1}). In the case of Ph$_2$-BDP-AlPorF$_3$ dyad, energy transfer from ^{1}AlPorF$_3$* to ^{1}(Ph$_2$-BDP)* was witnessed (k_{EnT} = 1.0 x 10^{10} s^{-1}), however, upon assembling the supramolecular triad, (Ph$_2$-BDP)-AlPorF$_3$←Im-C$_{60}$, electron transfer from ^{1}AlPorF$_3$* to C$_{60}$ (k_{CS} = 3.35 x 10^9 s^{-1}) followed by hole shift (k_{HS} = 1.00 x 10^9 s^{-1}) to Ph$_2$-BDP was witnessed. Finally, in the case of TPA$_2$-BDP-AlPorF$_3$←Im-C$_{60}$ triad, only electron transfer leading to (TPA$_2$-BDP)$^{+•}$-AlPorF$_3$←Im-(C$_{60}$)$^{-•}$ charge separated state and no energy transfer was observed. The facile oxidation of Ph$_2$-BDP and TPA$_2$-BDP compared to AlPorF$_3$ in the latter two triads facilitated charge separation through either an electron migration or hole transfer mechanism depending upon initial excitation. The charge-separated states in these triads persisted for about 20 ns.

Introduction

Conversion of sunlight energy into solar electricity or solar fuels (chemical energy) by using efficient and economically viable processes remain one of the challenges to mankind. In nature the photosynthetic system elegantly demonstrated the solar energy conversion into chemical energy by multi-step electron transfer reactions in which the initial charge separation is stabilized by a series of subsequent electron transfer steps that separate the two unpaired electrons. This way a high quantum yield of long-lived, light-induced charge separation is achieved. Ultimately, the generated high-energy stable radical pair utilized to perform nature's two fundamental reactions that are oxidation of water and reduction of CO$_2$.[1-4] In this perspective, there were many supramolecular multi-component donor-acceptor systems using different photo- and redox-active species have been reported and extensively studied to mimic and understand the mechanistic details of sequential energy and electron transfer reactions in natural photosynthesis with aim of solar energy conversion and storage.[5-19]

In many of these multi-component donor-acceptor systems porphyrins are commonly used as both optical and redox active component.[20-26] This is because porphyrins absorb light in visible region, moreover, their redox potentials and optical properties can be easily tuned by changing substituents on the periphery and/or the element in the centre of the porphyrin ring.[27, 28] These unique properties were exploited in combination with other redox and photoactive molecules to design a wide variety of donor-acceptor systems. In fact, porphyrin-based donor-acceptor systems have been shown as excellent models to understand the intricate details of energy and electron transfer mechanisms as well as factors that influence these processes. However, our knowledge of these factors and the ability to control them is currently far from complete. Moreover, most of these reaction centre model compounds are constructed along the horizontal plane of porphyrin, that is, the electron donor and acceptor lie in the same plane as the porphyrin ring, therefore the sequential electron transfer was studied along this plane.[8, 11, 18, 21, 29-36] In

[a.] Department of Chemistry & Biochemistry, University of Minnesota Duluth, 1039 University Drive, Duluth, Minnesota 55812, United States.
[b.] Department of Chemistry, University of North Texas, 1155 Union Circle, # 305070, Denton, Texas 76203-5017, United States.
+Electronic Supplementary Information (ESI) available: NMR spectroscopy, ESI mass, absorption and fluorescence titrations, cyclic voltammograms, TCSPC decay profiles and transient absorption spectra. See DOI: 10.1039/x0xx00000x

the natural reaction centers the chlorophylls are generally bound to the protein via axially ligation, often by histidine, and the axial ligands are important for controlling factors such as the free energy change and electronic coupling that govern electron transfer.[37] For artificial complexes, an added advantage of the axial arrangement is that the placement of the donor and acceptor units on opposite faces of the porphyrin ensures that they are spatially well separated and that unwanted interactions are minimized. Despite of these advantages, there are fewer number of systems designed and investigated to study the sequential electron transfer in perpendicular to the porphyrin plane.[38-44] This is mainly due to synthetic challenges, this arrangement is difficult to achieve with transition metal porphyrins, which often only allow for coordination of one axial ligand, and attachment of two different ligands via coordination bonds, is difficult to control. Hence, examples of step-wise or cascade electron transfer in such systems remain extremely rare. Another preferred property for an artificial reaction center model is the ability to capture the light at broader absorption window.[45-47] Most of the reported reaction center models are often limited in capturing the light due to narrow absorption bands. This can be addressed by incorporating multiple chromophores in artificial reaction center models to capture the entire visible spectrum. However, such models will require challenging synthetic routes moreover

the resulting energy states may not be favored for desired photoinduced processes.

In this context, here we report three novel broad band capturing vertically linked supramolecular triads, (BDP-AlPorF$_3$←Im-C$_{60}$, Ph$_2$-BDP-AlPorF$_3$←Im-C$_{60}$ and TPA$_2$-BDP-AlPorF$_3$←Im-C$_{60}$) comprised of aluminium(III) porphyrin (AlPorF$_3$), fullerene (C$_{60}$) and BODIPY derivative (BDP, BDP-Ph$_2$ or BDP-TPA$_2$, where BDP or BODIPY = borondipyrromethene, TPA = triphenylamine), see Schemes 1 and 2. The problem of attaching two different electron/energy transfer components axially is addressed by using main group metal porphyrin, aluminum(III) porphyrin, as it form axial covalent bonds with carboxylic acids resulting a 5-coordinate metal centre.[39-44, 48-52] Moreover, the high Lewis acidity of Al allows coordination by Lewis bases to form 6-coordinate complexes with the covalent ligand on one face of the porphyrin and the coordination bond on the opposite face.[39-44] Among the non-porphyrin molecules, BODIPY derivatives occupies a very special place as they have unique optical and redox properties. BODIPY derivatives have high fluorescence quantum yields, large extinction coefficients and have adequate excited lifetimes. Furthermore, they can act as an energy donor or electron donor depending on the other molecular component present in the donor-acceptor systems.[26, 45-47, 53-57]
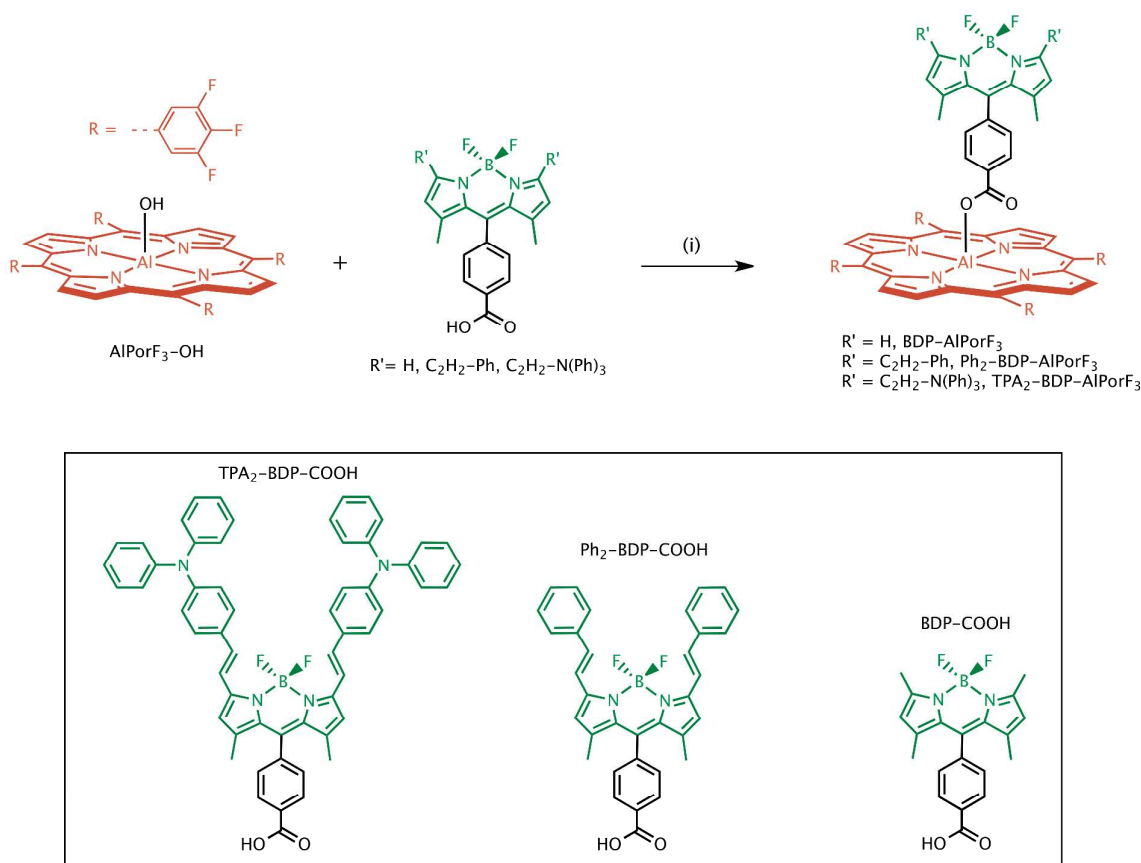
Scheme 1. Synthesis of investigated dyads, BDP-AlPorF$_3$, Ph$_2$-BDP-AlPorF$_3$ and TPA$_2$-BDP-AlPorF$_3$. Reaction conditions: (i) stirring in methanol and/or dichloromethane mixture for 12 h at room temperature under N$_2$.

Nanoscale

ARTICLE

Notably, the selected BODIPY derivatives (BDP, Ph₂-BDP and TPA₂-BDP) in this study possess a broad absorption profiles, that is, they absorb the light between 500 – 900 nm.[58] Additionally their redox properties were tailored by substitution of its peripheral positions.

On the other hand, as an electron acceptor fullerene (C_{60}) derivatives were widely employed in artificial photosynthetic model that is because after an electron accepting the charge delocalizes over the C_{60} dodecahedron and stabilizes the unpaired electron with minimum reorganization energy. The small reorganization energies of fullerenes in electron-transfer reactions result in fast charge separation and relatively slow charge recombination, yielding long-lived charge-separated states.[33, 59-62] By utilizing these unique properties of aluminium(III) porphyrin, C_{60} and BODIPY derivatives we designed and constructed three vertically linked broad band capturing supramolecular reaction centre models where photoinduced processes can be investigated in perpendicular direction to the porphyrin. Furthermore, these molecular triads are collectively capable of capturing light from the entire visible spectrum, consequently the newly designed reaction centres could remain photoactive throughout the visible region. The photoinduced energy and electron transfer process have been systematically investigated by using femtosecond transient absorption studies. We will show that the choice of photoinduced processes in the triads are strongly influenced by the nature of the BODIPY, and the stabilization of the charge separation by the BODIPY derivative is modest.

Experimental Section

Synthesis. All the chemicals and solvents were obtained from Sigma-Aldrich, Alfa Aesar or Fisher Chemicals and were used as received. Chromatographic materials were procured from Sigma-Aldrich or SiliCycle Inc. Synthesis of the precursor porphyrins such as 5,10,15,20-tetrakis(trifluoro phenyl)porphyrin (H_2PorF_3), and its aluminum(III) derivative 5,10,15,20-tetrakis(trifluorophenyl)porphyrinatoaluminum(III)
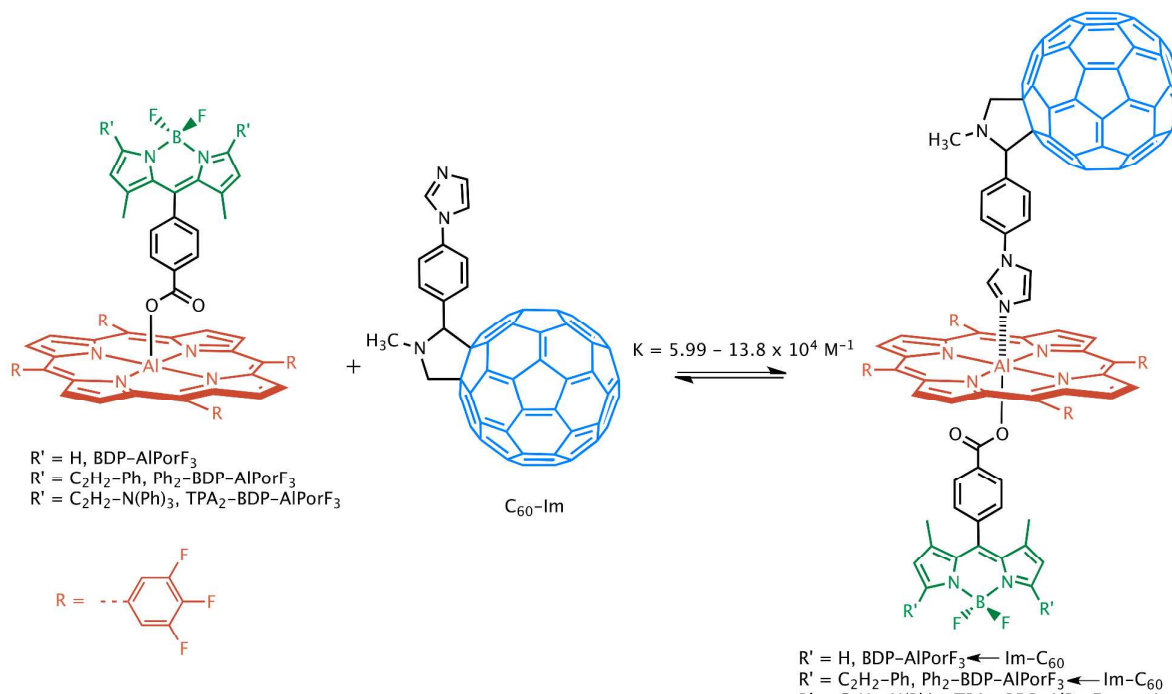
Scheme 2. The formation of self assembled triads, BDP-AlPorF₃←Im-C₆₀, Ph₂-BDP-AlPorF₃←Im-C₆₀, and TPA₂-BDP-AlPorF₃←Im-C₆₀, in non-coordinating *o*-dichlorobenzene or toluene.

Nanoscale

ARTICLE

hydroxide (AlPorF$_3$-OH), and the reference compound AlPorF$_3$-Ph (see Scheme 3) were synthesized according to the literature procedures.[63] Synthesis of BODIPY derivatives (BDP, Ph$_2$-BDP and TPA$_2$-BDP, see Scheme 1 for structural information) was reported elsewhere.[58]

Preparation of BDP-AlPorF$_3$. A mixture of AlPorF$_3$-OH (24 mg, 0.028 mmol) and BDP-COOH (10 mg, 0.024 mmol) in 5 mL of dry CH$_2$Cl$_2$:CH$_3$OH (= 4:1) was stirred at room temperature for 2 h under nitrogen. After reaction time the solvent was removed under reduced pressure and obtained product was washed with hot hexane yields the desired product in pure form. Yield: 31 mg (92%). ESI MS: m/z 1223.2557, 1175.2613 and 896.1347 for [M+H]$^+$, [M+H–BF$_2$]$^+$ and [M+CH$_3$CN–(BDP-COO)]$^+$ respectively, where M = C$_{64}$H$_{34}$AlBF$_{14}$N$_6$O$_2$. ^{1}H NMR (300 MHz, CDCl$_3$+drop of CD$_3$OD): δ, ppm 8.99 (m, 8H), 7.84 (m, 8H), 6.20 (d, 2H), 5.76 (s, 2H), 4.61 (d, 2H), 2.40 (s, 6H), 0.66 (s, 6H).

Preparation of Ph$_2$-BDP-AlPorF$_3$. A mixture of AlPorF$_3$-OH (20 mg, 0.023 mmol) and Ph$_2$-BDP-COOH (12.5 mg, 0.023 mmol) in 5 mL of dry CH$_2$Cl$_2$ was stirred at room temperature for 2 h under nitrogen followed by filtration through anhydrous

Na$_2$SO$_4$. The filtrate was collected and removed the solvent under reduced pressure and obtained product was washed with hot hexane yields the desired product in pure form. Yield: 30 mg (94%). FAB MS: m/z 1399.3309 and 896.1388 for [M+H]$^+$ and [M+CH$_3$CN–(Ph$_2$-BDP-COO)]$^+$, respectively, where M = C$_{78}$H$_{42}$AlBF$_{14}$N$_6$O$_2$. ^{1}H NMR (300 MHz, CDCl$_3$): δ, ppm 9.16 (s, 8H), 7.84 (m, 8H), 7.67 (m, 2H), 7.58 (d, 4H), 7.38 (t, 4H), 7.32 (t, 2H), 7.16 (d, 2H), 6.45 (s, 2H), 6.41 (d, 2H), 5.22 (d, 2H), 0.78 (s, 6H).

Preparation of TPA$_2$-BDP-AlPorF$_3$. A mixture of AlPorF$_3$-OH (21 mg, 0.024 mmol) and TPA$_2$-BDP-COOH (21 mg, 0.024 mmol) in 5 mL of dry CH$_2$Cl$_2$:CH$_3$OH (= 4:1) was stirred at room temperature for 2 h. After removal of the solvent, the mixture was washed with hot hexane yields the desired product in pure form. Yield: 40 mg (95%). FAB MS: m/z 1733.4841 and 896.1421 for [M]$^+$ and [M+CH$_3$CN–(TPA$_2$-BDP-COO)]$^+$, respectively, where M = C$_{102}$H$_{60}$AlBF$_{14}$N$_8$O$_2$. ^{1}H NMR (300 MHz, CDCl$_3$): δ, ppm 9.16 (s, 8H), 7.84 (m, 8H), 7.50 (m, 2H), 7.41 (d, 4H),7.26 (m, 8H), 7.13 (m, 10H), 7.07 (t, 4H), 6.99 (d, 4H), 6.40 (m, 4H), 5.25 (d, 2H), 0.77 (s, 6H).

Scheme 3. Formation of self-assembled dyad, Ph-AlPorF$_3$←Im-C$_{60}$, in o-dichlorobenzene or toluene.
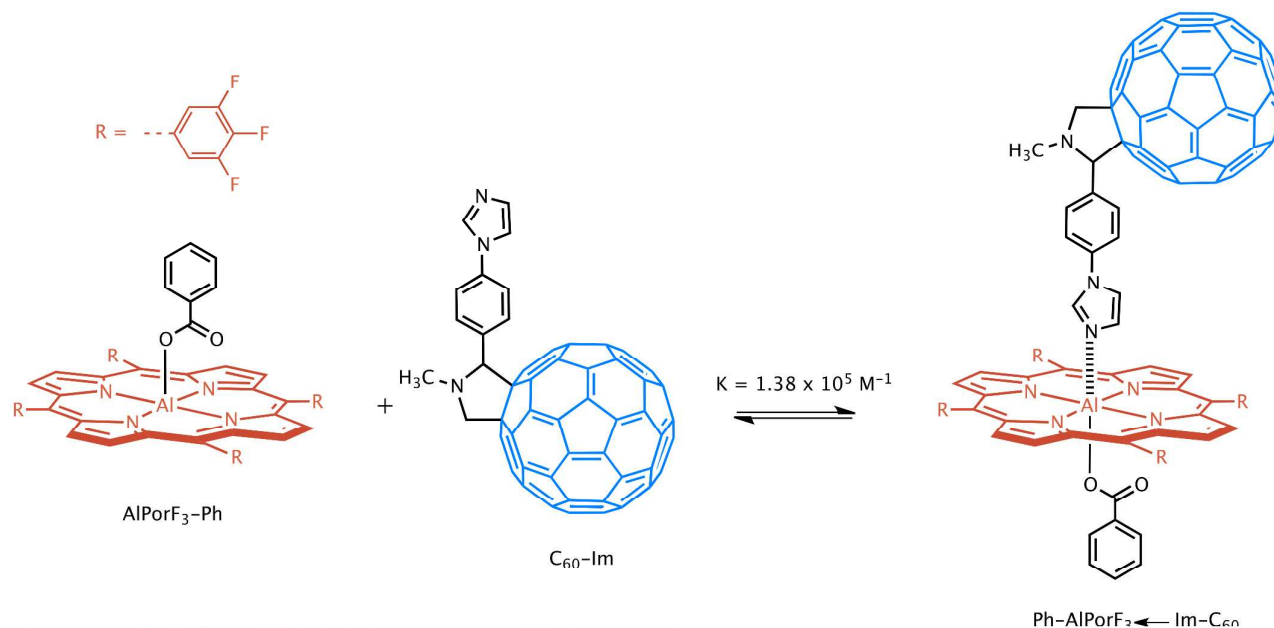
Methods.

NMR and mass spectroscopy. NMR spectra were recorded with Bruker Avance 300 MHz and Varian 500 MHz NMR spectrometer using CDCl$_3$ and/or CD$_3$OD as the solvents. ESI

mass spectra were recorded on a Bruker MicroTOF-III mass spectrometer.

Electrochemistry. Cyclic and differential pulse voltammetric experiments (*o*-dichlorobenzene, 0.1 M tetrabutylammonium perchlorate, (TBAP) were performed on a BAS Epsilon electrochemical analyzer (working: glassy carbon, auxiliary electrodes: Pt wire, reference electrode: Ag wire). The Fc^+/Fc (Fc = ferrocene) couple was used to calibrate the redox potential values.

Absorption and fluorescence spectroscopy. The UV/Vis spectra were recorded with the Agilent Cary 100 UV-VIS spectrophotometer. Concentration of the samples used for these measurements ranged from 1×10^{-6} M (porphyrin Soret and BDP derivative bands) to 5×10^{-5} M (Q-bands) solutions. Steady-state fluorescence spectra were recorded using a Photon Technologies International Quanta Master 8075-11 spectrofluorimeter, equipped with a 75 W xenon lamp, running with FelixGX software.

Absorption and fluorescence titrations. Absorption titrations were carried out in *o*-dichlorobenzene (*o*-DCB) at concentrations appropriate for measuring the porphyrin Soret band. A solution containing $AlPorF_3$ derivative (BDP-$AlPorF_3$, Ph_2-BDP-$AlPorF_3$, TPA_2-BDP-$AlPorF_3$ or $AlPorF_3$-Ph) was placed in a cuvette and titrated by adding aliquots of a concentrated solution of the C_{60}-Im (or Me-Im). The C_{60}-Im (or Me-Im) solution also contained the $AlPorF_3$ derivative at its initial concentration so that the porphyrin concentration remained constant throughout the titration. The binding constants were calculated using the Benesi-Hildebrand equation,[64] [D]/Abs = $(1/[A])(1/\varepsilon K) + (1/\varepsilon)$, where, [D] is the total concentration of bound and unbound donor and is kept fixed, Abs is the absorption of complex at the wavelength λ, [A] is the total concentration of the C_{60}-Im (or Me-Im) which is varied, *K* is binding constant and ε is the molar absorptivity of complex. In an analogous manner, steady-state fluorescence titrations were carried out in *o*-DCB using solutions at constant concentration of $AlPorF_3$ derivative and varying concentration of C_{60}-Im (or Me-Im). The solutions were excited at the isosbestic point wavelength, which was obtained from the corresponding absorption titrations. The estimated error in K values is $\pm 12\%$.

Femtosecond transient absorption spectroscopy. Femtosecond transient absorption spectroscopy experiments were performed using an Ultrafast Femtosecond Laser Source (Libra) by Coherent incorporating diode-pumped, mode locked Ti:Sapphire laser (Vitesse) and diode-pumped intracavity doubled Nd:YLF laser (Evolution) to generate a compressed laser output of 1.5 W. For optical detection, a Helios transient absorption spectrometer provided by Ultrafast Systems LLC coupled with an optical parametric amplifier (OPA) provided by Light Conversion was used. The source for the pump and probe pulses were derived from the fundamental output of Libra (Compressed output 1.5 W, pulse width 100 fs) at a

repetition rate of 1 kHz. 95% of the fundamental output of the laser was introduced into the OPA, while the rest of the output was used for generation of the white light continuum. In the present study, the maximum absorption wavelength for each compound was used in all the experiments. Kinetic traces at appropriate wavelengths were assembled from the time-resolved spectral data. Data analysis was performed using Surface Xplorer software supplied by Ultrafast Systems. All measurements were conducted in degassed solutions at 298 K.

Results and Discussions

Synthesis. The synthesis details of the investigated compounds are given in the Schemes 1, 2 & 3. The porphyrin was tethered with 3,4,5-trifluorophenyl units on the *meso*-positions to make the potentials more positive. This is not only provides sufficient driving force for the charge separation through both an electron migration or hole transfer between selected photo and redox units (at least in the case of triads Ph_2-BDP-$AlPorF_3 \leftarrow$ Im-C_{60} and TPA_2-BDP-$AlPorF_3 \leftarrow$ Im-C_{60}) but also it ensures the electron flow towards C_{60}. On the other hand, the selected BODIPY derivatives (BDP, Ph_2-BDP, and TPA_2-BDP) guarantee the panchromatic effect in the entire visible range in combination with porphyrin entity. Briefly, the new dyads (BDP-$AlPorF_3$, Ph_2-BDP-$AlPorF_3$, TPA_2-BDP-$AlPorF_3$) were prepared by condensation of $AlPorF_3$-OH with BDP derivative (BDP-COOH, Ph_2-BDP-COOH or TPA_2-BDP-COOH) in quantitative yields, Scheme 1. The structural characterization of the porphyrins was performed by various spectroscopic techniques, see the experimental section and supporting information for details. Lewis acid-base interactions, between imidazole appended C_{60} and Al centre of $AlPorF_3$, were exploited to construct the triads, BDP-$AlPorF_3 \leftarrow$ Im-C_{60}, Ph_2-BDP-$AlPorF_3 \leftarrow$ Im-C_{60} and TPA_2-BDP-$AlPorF_3 \leftarrow$ Im-C_{60} (see Scheme 2), and its corresponding self-assembled dyad Ph-$AlPorF_3 \leftarrow$ Im-C_{60} (see Scheme 3). Absorption and fluorescence titrations were used to monitor the formation of triads.

UV−visible absorption spectroscopy. The UV−visible spectra of BDP-$AlPorF_3$, Ph_2-BDP-$AlPorF_3$, TPA_2-BDP-$AlPorF_3$ and its reference compounds, $AlPorF_3$-Ph and BDP derivative (BDP-COOH, Ph_2-BDP-COOH or TPA_2-BDP-COOH), were measured in dichloromethane and the spectra are shown in Figure 1. The band positions (Q-band and B-band) and their molar extinction coefficients are summarized in Table 1. As shown in Figure 1 and Table 1, the absorption spectrum of the dyad is essentially a linear combination of its reference porphyrins. Furthermore, the band positions and molar extinction coefficients (ε) of the dyad are similar to corresponding monomeric units. Overall, the absorption studies suggest that there exist no or
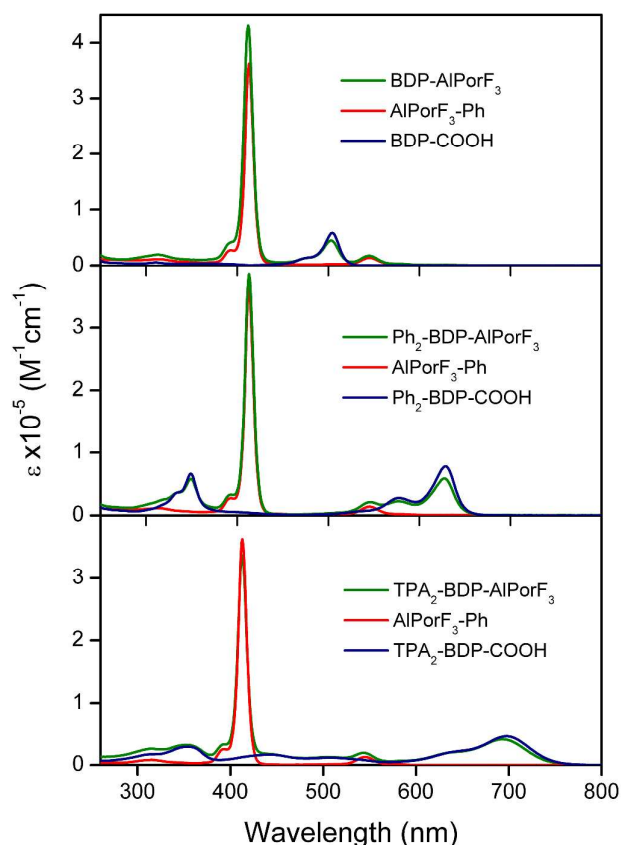
Figure 1. UV–visible absorption spectra of newly investigated dyads and their corresponding reference compound in CH_2Cl_2.

weak interactions between basal porphyrin ($AlPorF_3$) and axial BDP derivative (TPA_2-BDP, Ph_2-BDP, and BDP), attributed to their perpendicular orientation which decreases the electronic coupling between their respective π-systems. The imidazole-appended fullerene, C_{60}-Im, has relatively weak and very broad absorption bands in ultraviolet region.[6] Based on constituent absorption profiles of dyads, 545 nm wavelength was used to excite the $AlPorF_3$ whereas to 500, 630 and 700 nm wavelengths were used to excite the BDP, Ph_2-BDP or TPA_2-BDP, respectively. However, there is a significant overlap between BDP derivative and $AlPorF_3$ absorption profiles.

Therefore, the exclusive excitation of $AlPorF_3$ or BDP derivative is not feasible under our experimental conditions.

Scheme 2 illustrates the formation of the investigated triads from its reference compounds and was monitored by absorption and fluorescence spectroscopy. Figure 2a shows absorption titrations of TPA_2-BDP-$AlPorF_3$ vs C_{60}-Im in o-DCB. Upon addition of C_{60}-Im, the porphyrin bands 418, 546 and 588 nm are shifted to 428, 561 and 600 nm, respectively. Isosbestic points are observed at 423 and 555 nm, indicating the formation of the supramolecular self-assembled triad, TPA_2-BDP-$AlPorF_3$←Im-C_{60}. The shifts in the porphyrin bands are typical of axial coordination of nitrogen-based (e.g. pyridine or imidazole) ligands to AlPors.[39-41, 43, 44, 49-51, 63] Benesi−Hildebrand analysis[64] (Figure 2a, inset) gives a linear plot indicating that a 1:1 complex is formed, and the slope yields a binding constant (K) 8.8×10^4 M^{-1}. Similar spectral changes and binding constants were observed in titrations of BDP-$AlPorF_3$ vs C_{60}-Im (Figure S5), Ph_2-BDP-$AlPorF_3$ vs C_{60}-Im (Figure S7) and $AlPorF_3$-Ph vs C_{60}-Im (Figure 3) as well as control titrations BDP-$AlPorF_3$ vs Me-Im (Figure S6), Ph_2-BDP-$AlPorF_3$ vs Me-Im (Figure S8), TPA_2-BDP-$AlPorF_3$ vs Me-Im (Figure S9) and $AlPorF_3$-Ph vs Me-Im (Figure S10). The obtained binding constants are summarized in Table 2. Interestingly, the observed binding constants are found to be one order magnitude higher than previously reported values.[40, 63] This is because: (i) the Al centre in investigated porphyrin acts as a much better Lewis acid due to the presence of electron withdrawing 3,4,5-trifluorophenyl substitution in the meso-positions of porphyrin and (ii) imidazole is much better Lewis base than pyridine. Together with strong Lewis acidity and basicity results the higher binding constants in present compounds. Absorption studies also can be employed to quantify any possible electronic interaction between $AlPorF_3$ and BDP derivatives (or C_{60}) entities. The absence of any additional bands in these titrations suggests that perturbation of the electronic structures of the photo- and redox-active components due to the formation of the complex is relatively small. However, compared to covalent attachment (of BDP derivative) axial coordination (of imidazole appended C_{60}) causes a greater perturbation of the porphyrin.

Nanoscale

ARTICLE
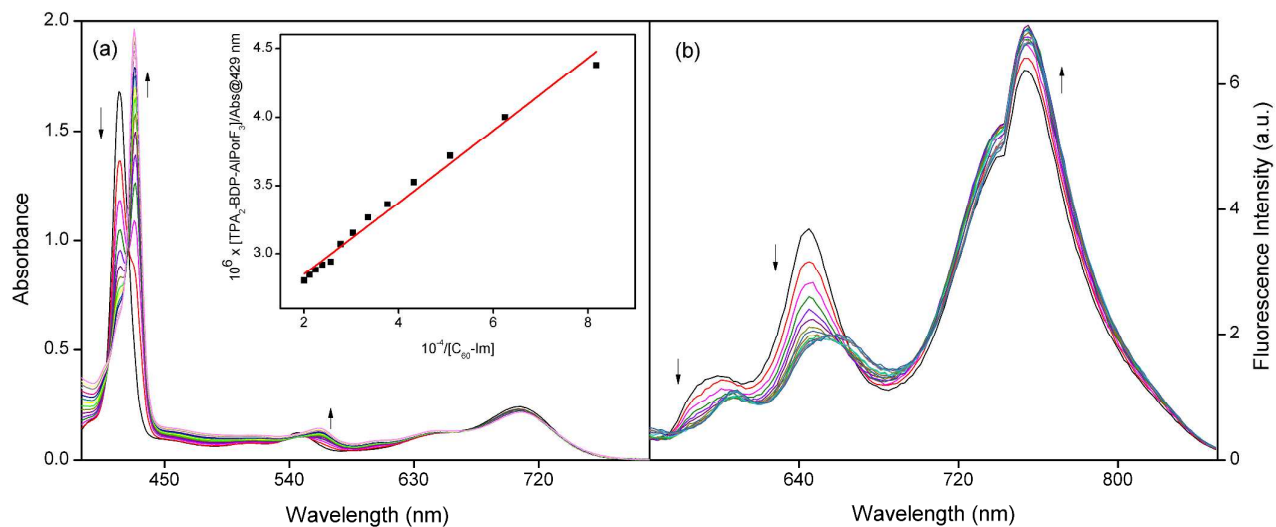
Figure 2. (a) Absorption and (b) fluorescence titrations of TPA$_2$-BDP-AlPorF$_3$ vs C$_{60}$-Im in o-DCB. The inset shows the Benesi–Hildebrand plot of the absorbance change at 429 nm. The excitation wavelength was chosen at the isosbestic point, 555 nm, obtained from UV-visible titrations. In titrations, C$_{60}$-Im was added up to 4.23 × 10^{-6} M in 20 µl (2.16 × 10^{-4} M) increments to a 1 ml (5.5 × 10^{-6} M) solution of TPA$_2$-BDP-AlPorF$_3$.
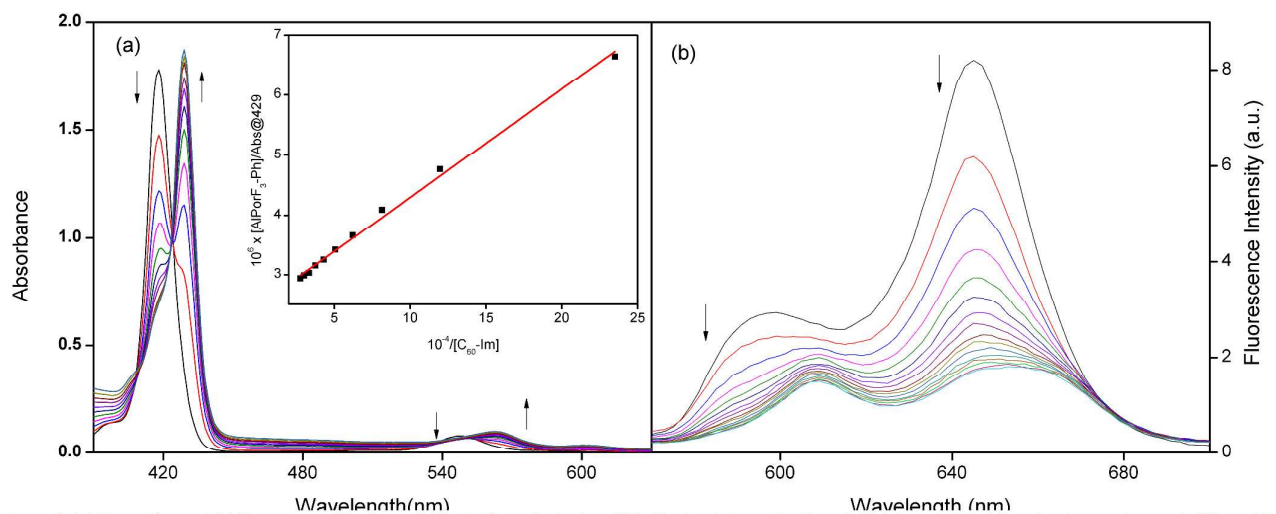
Figure 3. (a) Absorption and (b) fluorescence titrations of AlPorF$_3$ Ph vs C$_{60}$ Im in o DCB. The inset shows the Benesi–Hildebrand plot of the absorbance change at 429 nm. The excitation wavelength was chosen at the isosbestic point, 555 nm, obtained from UV-visible titrations. In titrations, C$_{60}$-Im was added up to 4.3 × 10^{-6} M in 20 µl (2.17 × 10^{-4} M) increments to a 1 ml (5.5 × 10^{-6} M) solution of AlPorF$_3$-Ph.

Nanoscale

ARTICLE

Table 1. Absorption (in CH_2Cl_2) and redox (in *o*-DCB, 0.1 M TBAP) data of investigated compounds.

Sample	Potential [V *vs* Fc]		Absorption
	Oxidation	Reduction	λ_{max} [nm] (log ε [M^{-1} cm^{-1}])
TPA$_2$-BDP-AlPorF$_3$	0.14, 0.28, 0.52	−1.54, −1.92	314 (4.42), 352 (4.51), 443 (4.24), 504 (4.11), 543 (4.29), 638 (4.31), 693 (4.62)
Ph$_2$-BDP-AlPorF$_3$	0.55	−1.49, −1.90	349 (4.76), 413 (5.59), 546 (4.33), 577 (4.35), 627 (4.77)
BDP-AlPorF$_3$	0.55, 0.80	−1.52, −1.74, −1.93	313 (4.29), 412 (5.63), 503 (4.65), 544 (4.24)
AlPorF$_3$-Ph	0.54, 0.88	−1.55, −1.93	314 (4.06), 413 (5.56), 546 (4.14)
TPA$_2$-BDP-COOH	0.13, 0.27, 0.51	−1.53	311 (4.23), 354 (4.47), 444 (4.22), 507 (4.07), 638 (4.32), 698 (4.66)
Ph$_2$-BDP-COOH	0.47	−1.47	349 (4.82), 577 (4.44), 628 (4.89)
BDP-COOH	0.79	−1.73	311 (3.74), 504 (4.77)
C$_{60}$-Im[a]	-	−1.13, −1.51, −2.05	255 (5.25), 308 (4.73)

[a]Reduction potentials were adapted from literature.[6]

Table 2. The obtained binding constants from Benesi−Hildebrand analysis of various titration of investigated compounds in *o*-DCB.

Titration	$K (M^{-1})$
AlPorF$_3$-Ph *vs* C$_{60}$-Im	1.38×10^5
AlPorF$_3$-Ph *vs* Me-Im	3.92×10^5
BDP-AlPorF$_3$ *vs* C$_{60}$-Im	1.03×10^5
BDP-AlPorF$_3$ *vs* Me-Im	2.96×10^5
Ph$_2$-BDP-AlPorF$_3$ *vs* C$_{60}$-Im	5.99×10^4
Ph$_2$-BDP-AlPorF$_3$ *vs* Me-Im	1.24×10^5
TPA$_2$-BDP-AlPorF$_3$ *vs* C$_{60}$-Im	8.81×10^4
TPA$_2$-BDP-AlPorF$_3$ *vs* Me-Im	2.19×10^5

estimated error: K ± 12%

Electrochemistry. Cyclic voltammetry of the newly investigated compounds was measured in 0.1 M TBAP/*o*-DCB with ferrocene as an internal standard. Representative voltammograms are shown in Figure S11, and the data is summarized in Table 1. The redox processes of all the compounds are found to be one-electron reversible based on the peak-to-peak separation values, and the cathodic-to-anodic peak current ratio. The voltammogram of the dyads is essentially a sum of the voltammograms of its reference monomers. For example, the voltammogram of TPA$_2$-BDP-AlPorF$_3$ is the combination of its monomers AlPorF$_3$-Ph and TPA$_2$-BDP-COOH. During the cathodic scan, the dyad showed two reduction processes at −1.54 and −1.92 V *vs* Fc. On the basis of the respective monomers, the observed first process is assigned to the combination of first reduction of AlPorF$_3$ and TPA$_2$-BDP units, whereas the second process is assigned to the second reduction of the AlPorF$_3$ unit. The anodic scan reveals three oxidation processes for the dyad at 0.14, 0.28 and 0.52 V. The first two processes are assigned to the oxidation of axial TPA$_2$-BDP unit, and third process belongs to the combination of first oxidation of AlPorF$_3$ and third oxidation of axial TPA$_2$-BDP unit. As anticipated, the dyad showed a combination of processes from their respective monomeric porphyrin units without any perturbation in their redox potentials. Therefore, the observed cyclic voltammograms and redox data suggest that the components of the dyad do not influence one another significantly. Similar results were observed from the dyads, BDP-AlPorF$_3$ and Ph$_2$-BDP-AlPorF$_3$. The redox potentials of C$_{60}$-Im were adapted from the literature,[6] which showed three processes corresponding to the its consecutive reduction of the C$_{60}$ moiety. Further, the cyclic voltammetry studies performed to investigate the influence of C$_{60}$-Im on the redox properties of dyad, that is during the formation of triad molecules. As anticipated there were no significant changes found in redox potentials of components of the triad molecules and are consistent with UV-visible studies.

Energy level diagrams. The redox potentials are used in combination with optical data to construct the energy level

diagram of the states involved in possible electron-transfer processes. Figure 4 summarizes the energy levels of the investigated compounds. For these calculations, we have ignored the stabilization energy due to the Coulomb interaction of the charges. The energy of the lowest excited state (E_{0-0}) of the $AlPorF_3$ unit has been estimated from the position of the blue edge of the fluorescence spectrum at 579 nm (= 2.14 eV). The energies of the lowest excited singlet state (= 1.75 eV) and triplet state (= 1.50 eV) of C_{60} as well as the triplet state energies (= 1.61 eV) of $AlPorF_3$ have been taken from the literature.[63] Also, the singlet energy of excited singlet state being, 2.43 eV for BDP, 1.94 eV for Ph_2-BDP, and 1.73 eV for TPA_2-BDP.[58] The redox potentials can be used to estimate the energy of the charge-separated state E_{CS} (relative to the ground state) and the free-energy changes for charge separation (ΔG_{CS}), hole stabilization (ΔG_{HS}) and electron migration (ΔG_{EM}) using the Rehm and Weller method,[65-67]

$$\Delta G_{CS} = E_{CS} - E_{0-0} \qquad (1)$$

$$\Delta G_{HS/EM} = E_{CS1} - E_{CS2} \qquad (2)$$

where E_{CS} is the difference between the first oxidation of electron donor and the first reduction of electron acceptor. The calculated free-energy level diagrams suggest the following electron transfer processes are energetically favourable in the triads (Ph_2-BDP-$AlPorF_3 \leftarrow Im$-C_{60} and TPA_2-BDP-$AlPorF_3 \leftarrow Im$-C_{60}) upon excitation of $AlPorF_3$: (i) oxidative electron transfer from the excited singlet state of $AlPorF_3$ ($^1AlPorF_3^*$) to fullerene followed by hole shift to BDP unit, or (ii) reductive electron transfer from BDP derivative (Ph_2-BDP and TPA_2-BDP) to $^1AlPorF_3^*$ followed by a charge shift to C_{60}. In the case of dyad, BDP-$AlPorF_3$, either of the oxidative and reductive electron transfer processes are energetically not favourable upon excitation of $AlPorF_3$. However, upon BDP entity excitation, the oxidative electron transfer is energetically favourable in all the three investigated triads.

Steady-state fluorescence studies. The steady-state fluorescence spectra of the dyads BDP-$AlPorF_3$, Ph_2-BDP-$AlPorF_3$ and TPA_2-BDP-$AlPorF_3$ and its reference compounds $AlPorF_3$-Ph and BDP derivatives were measured in o-DCB (Figures 5 – 7) and toluene (Figures S13-S15). Very similar trends were observed in both solvents, suggest that the solvent polarity has a little influence on the excited state properties. The experiments were carried out at the same concentration of each sample. Two different excitation wavelengths were used to study the photoinduced processes. The wavelength of 545 nm used to excite the porphyrin Q-band, whereas the wavelengths 500, 610 and 700 nm were used to excite the BDP moiety in the dyads BDP-$AlPorF_3$, Ph_2-BDP-$AlPorF_3$ and TPA_2-BDP-$AlPorF_3$, respectively. The fluorescence lifetimes of the probes were measured using time correlated single photon counting technique (TCSPC) in toluene. $AlPorF_3$-Ph and BDP derivatives revealed monoexponential decay with lifetime of 3.37 ns for $AlPorF_3$-Ph, 3.36 ns for BDP, 4.06 ns for Ph_2-BDP

and 3.16 ns for TPA_2-BDP, respectively (see Figure S12 for representative decay profiles).
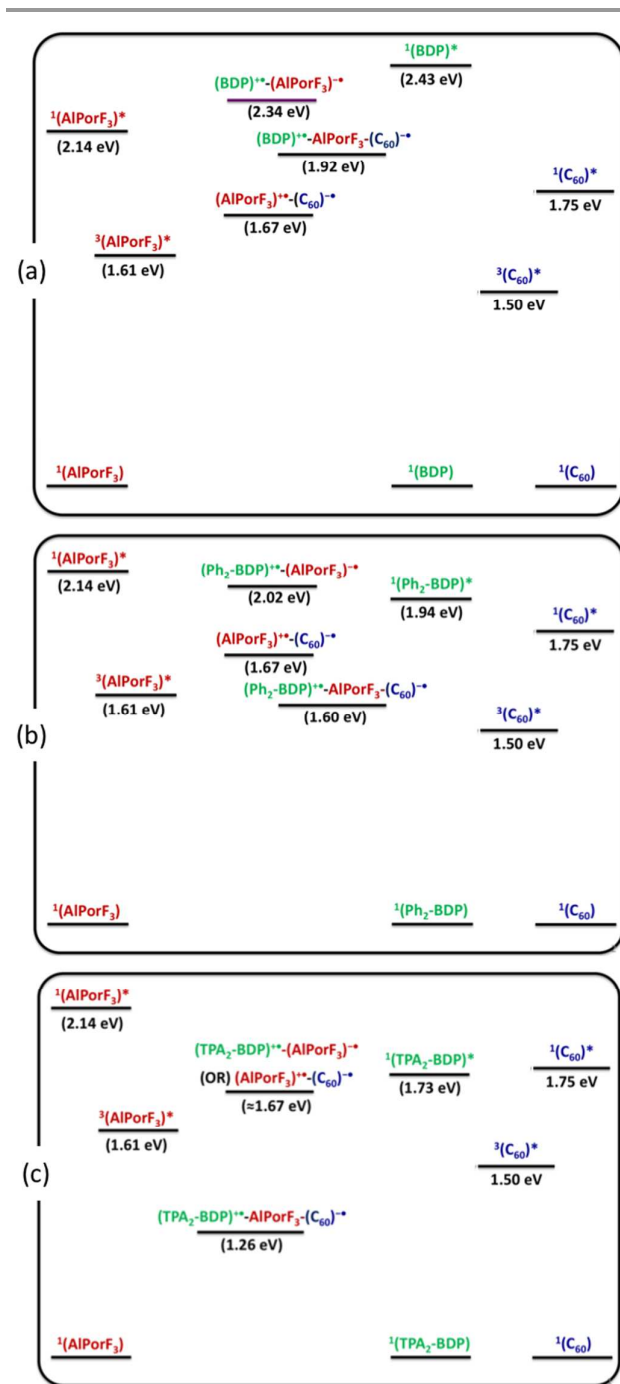
Figure 4. Energy level diagram of (a) BDP-$AlPorF_3 \leftarrow Im$-C_{60}, (b) Ph_2-BDP-$AlPorF_3 \leftarrow Im$-C_{60} and (c) TPA_2-BDP-$AlPorF_3 \leftarrow Im$-C_{60} in o-DCB.

BDP-$AlPorF_3 \leftarrow Im$-C_{60}: The quantitative fluorescence spectra of BDP-$AlPorF_3$ and its reference compounds are measured in o-DCB and toluene and were shown in Figure 5 and Figure S13, respectively. Upon excitation of porphyrin at 545 nm

(where light is exclusively absorbed by $AlPorF_3$), it was found that the fluorescence band maxima (590 and 645 nm) and fluorescence intensity of dyad are quite close to those of its reference compound $AlPorF_3$-Ph, Figure 5a. The observed results suggest that the excited $AlPorF_3$ relax back to its ground state without any additional photoinduced processes. This observation is consistent with the energy level diagram where neither the energy transfer nor the electron transfer from $^1(AlPorF_3)^*$ to BDP derivative is energetically favourable. In contrast, excitation of BDP moiety at 500 nm (where 92% light is absorbed by BDP) resulted in a strong quenching (~82%) in fluorescence of BDP (520 nm) in the dyad, see Figure 6b. This could be due to singlet-singlet energy transfer from $^1BDP^*$ to $^1(AlPorF_3)^*$ as there is a significant spectral overlap between BDP emission and $AlPorF_3$ absorption profiles, see Figures 5b & 1(top). To test this hypothesis, excitation spectrum was collected for the dyad BDP-$AlPorF_3$ in o-DCB. Figure 5b-inset shows the corrected excitation spectrum of the dyad in o-DCB collected at 660 nm (emission monochromator) where only the $AlPorF_3$ emits. Overlap of the corrected and normalized excitation spectra with the corresponding absorption spectra revealed a strong singlet−singlet energy transfer (~82%) from $^1BDP^*$ to $^1AlPorF_3^*$. Although, the singlet-singlet energy transfer is a main quenching mechanism, electron transfer from $^1BDP^*$ to $AlPorF_3$ moiety cannot be rule out as this process is energetically favourable, and the ΔG_{CS} for this process is estimated to be −0.09 eV.

Figure S5b shows the titration of BDP-$AlPorF_3$ with C_{60}-Im in o-DCB, the excitation wavelength was chosen at the isosbestic point, 555 nm, which was obtained from UV-visible titrations. As shown in Figure S5b, a strong quenching is accompanied by red shift (590 and 645 nm to 609 and 661 nm) in $AlPorF_3$ fluorescence bands. These spectral changes confirm the formation of triad, BDP-$AlPorF_3$←Im-C_{60}. However, to investigate the possible quenching mechanism several control experiments were carried out. When BDP-$AlPorF_3$ is titrated with Me-Im, lacking the C_{60}, primarily a red shift of the fluorescence bands with increase in intensity (see Figure S6b) was observed. The increase in intensity is due to changes in the intrinsic fluorescence rates as a result of structural modifications when imidazole coordinates to Al centre. Whereas, titration of $AlPorF_3$-Ph with C_{60}-Im (i.e. the formation of self-assembled dyad Ph-$AlPorF_3$←Im-C_{60}, see Scheme 3) leads to a red shift with a strong quenching in fluorescence, see Figure 3b. From this, we conclude that the red shift is due to coordination of imidazole whereas the fluorescence quenching is due an intramolecular electron transfer from $^1(AlPorF_3)^*$ to C_{60} moiety to yield BDP-$(AlPorF_3)^{+\bullet}$←Im-$(C_{60})^{\bullet-}$. The corresponding ΔG_{CS} for this process is estimated to be −0.47 eV. However, the subsequent hole-shift, i.e. BDP-$(AlPorF_3)^{+\bullet}$←Im-$(C_{60})^{-\bullet}$ to $(BDP)^{+\bullet}$-

$AlPorF_3$←Im-$(C_{60})^{-\bullet}$, is unlikely to take place because it is an endergonic process, see Figure 4a.

Ph_2-BDP-$AlPorF_3$←Im-C_{60}: The fluorescence spectra of Ph_2-BDP-$AlPorF_3$ dyad and its reference compounds in o-DCB and toluene are shown in Figures 6a and S14, respectively. Upon excitation of the dyad at 545 nm (where 64% light is absorbed by $AlPorF_3$) resulted the fluorescence bands at 583, 643 and 701 nm. Based on its reference compounds the observed first two bands are combination of $AlPorF_3$-Ph and Ph_2-BDP-COOH. To quantify the quenching efficiency, intensity of the 583 nm band was considered and found to be ~54%. In contrary, the intensity of 643 and 701 nm bands increased with respect to Ph_2-BDP. These spectral changes could be due to singlet-singlet energy transfer, which is supported by significant spectral overlap between the fluorescence spectrum of $AlPorF_3$ and absorption spectrum of Ph_2-BDP moiety (Figures 6a & 1(middle)). This was further investigated by using the fluorescence excitation spectrum. Figure 6a-inset shows the corrected excitation spectrum of the dyad in o-DCB collected at 720 nm (emission monochromator) where only the Ph_2-BDP emits. Overlap of the corrected and normalized excitation spectra with the corresponding absorption spectra revealed that the singlet−singlet energy transfer (EnT) efficiency is 42% for the dyad in o-DCB. The remaining 12% quenching could be attributed to the electron transfer (ET) from Ph_2-BDP to $^1(AlPorF_3)^*$ as the Gibbs free energy change (ΔG_{CS}) for this process was found to be exergonic (−0.12 eV). Furthermore, excitation of the dyad at 630 nm (where 99% of light is absorbed by Ph_2-BDP showed bands 642 and 698 nm exclusively due to the Ph_2-BDP component in the region, and its intensity was found to be similar to the sum of the calculated spectrum of Ph_2-BDP and $AlPorF_3$-Ph. Thus, we conclude that the electron transfer from $^1(Ph_2$-BDP$)^*$ to $AlPorF_3$ is weak or negligible, though the corresponding ΔG_{CS} is estimated to be −0.34 eV.

Figure S7b shows the fluorescence spectra of the Ph_2-BDP-$AlPorF_3$ dyad with increasing amounts of imidazole-appended fullerene (C_{60}-Im). The excitation wavelength was adjusted to the isosbestic point at 556 nm. Upon addition of C_{60}-Im, the fluorescence intensity decreases which supports the formation of a coordination complex, Ph_2-BDP-$AlPorF_3$←Im-C_{60}. As discussed in the previous section, the observed decrease in the fluorescence is due to electron transfer from $^1(AlPorF_3)^*$ to C_{60} to yield a first charge separated state Ph_2-BDP-$(AlPorF_3)^{+\bullet}$←Im-$(C_{60})^{\bullet-}$. Based on the energy level diagram, Figure 4b, the resulting Ph_2-BDP-$(AlPorF_3)^{+\bullet}$←Im-$(C_{60})^{-\bullet}$ state in principle can undergo a hole-shift process to form a second charge separated state $(Ph_2$-BDP$)^{+\bullet}$-$AlPorF_3$←Im-$(C_{60})^{-\bullet}$ as the ΔG_{HS} for this process is estimated to be −0.34 eV.

Nanoscale

ARTICLE
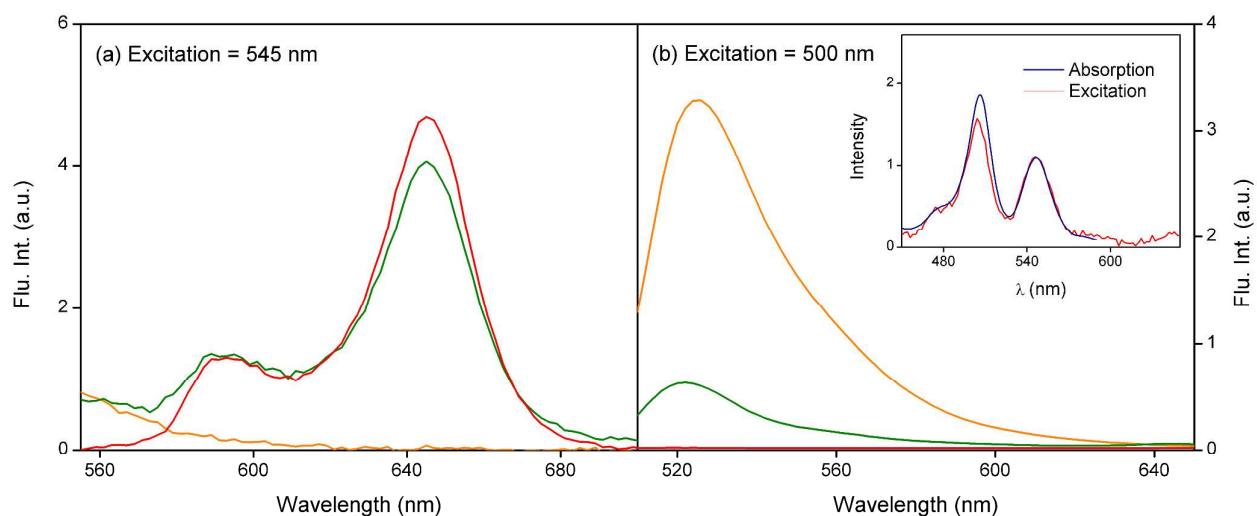
Figure 5. Steady-state fluorescence spectra of the dyad BDP-AlPorF$_3$ (green)), AlPorF$_3$-Ph (red) and BDP-COOH (orange) in *o*-DCB: (a) at 545 nm and (b) at 500 nm. Inset: Absorption (blue) and corrected fluorescence excitation (red) spectra of dyad in *o*-DCB. The spectra were normalized between 525 and 575 nm.
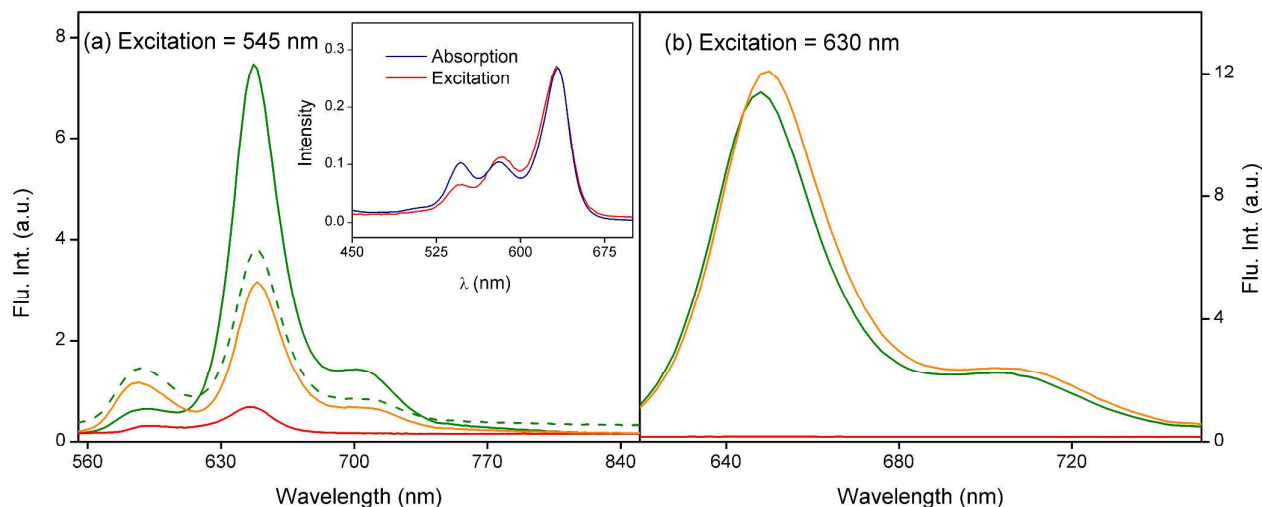
Figure 6. Steady-state fluorescence spectra of the dyad Ph$_2$-BDP-AlPorF$_3$ (green), calculated mixture of AlPorF$_3$-Ph and Ph$_2$-BDP-COOH (*green dotted*), AlPorF$_3$-Ph (red) *and* Ph$_2$-BDP-COOH (orange) in *o*-DCB: (a) at 545 nm and (b) at 630 nm. Inset: Absorption (blue) and corrected fluorescence excitation (red) spectra of Ph$_2$-BDP-AlPorF$_3$ in o-DCB. The spectra were normalized between 600 and 675 nm.

Nanoscale

ARTICLE
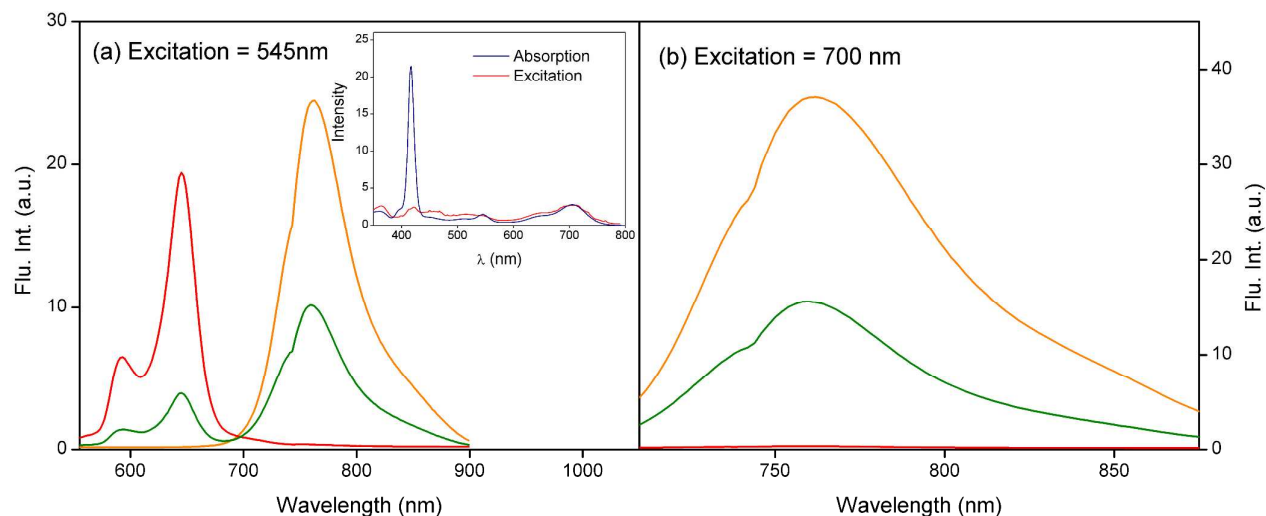
Figure 7. Steady-state fluorescence spectra of the dyad TPA$_2$-BDP-AlPorF$_3$ (green), AlPorF$_3$-Ph (red) and TPA$_2$-BDP-COOH (orange) in *o*-DCB: (a) at 545 nm and (b) 700 nm. Inset: Absorption (blue) and corrected fluorescence excitation (red) spectra of TPA$_2$-BDP-AlPorF$_3$ in *o*-DCB. The spectra were normalized between 650 and 800 nm.

TPA$_2$-BDP-AlPorF$_3$←Im-C$_{60}$: Figures 7 and S15 show the fluorescence spectra of the triad and its reference compounds in *o*-DCB. Upon excitation of porphyrin at 545 nm (where ~62% light is absorbed by the AlPorF$_3$), results in the appearance of fluorescence bands due to AlPorF$_3$ (bands at 585 and 643 nm) and TPA$_2$-BDP (broad band cantered at 727 nm) components. It was found that the fluorescence band maxima of AlPorF$_3$ and TPA$_2$-BDP components are quite close to those of AlPorF$_3$-Ph or TPA$_2$-BDP-COOH, respectively. However, the fluorescence intensity of the AlPorF$_3$ component is strongly quenched (~80%, emission monitored at 585 nm) in comparison with that of the reference compound AlPorF$_3$-Ph. The observed results clearly suggest that the ^{1}(AlPorF$_3$)* state is being strongly quenched by TPA$_2$-BDP. The possibility of energy transfer is supported by a significant spectral overlap between the emission spectrum of AlPorF$_3$ and absorption spectrum of TPA$_2$-BDP (Figures 7a & 1(bottom)). Figure 7a-inset shows the corrected excitation spectrum of the dyad in *o*-DCB collected at 800 nm (emission monochromator) where only the TPA$_2$-BDP emits. Overlap of the corrected and normalized excitation spectra with the corresponding absorption spectra revealed that the singlet−singlet energy transfer (EnT) is negligible for the dyad. Therefore, the observed quenching could be solely attributed to the electron transfer (ET) from TPA$_2$-BDP to ^{1}(AlPorF$_3$)* as the ΔG_{CS} for this process is found to be exergonic (−0.47 eV). Furthermore, excitation of the dyad at 700 nm (where light is absorbed exclusively by TPA$_2$-BDP)

showed a band exclusively due to the TPA$_2$-BDP component in the 727 nm region, and its intensity found to be quenched (~60%) with respect to the TPA$_2$-BDP-COOH. The fact that there is an insignificant overlap between TPA$_2$-BDP emission and AlPorF$_3$ absorption we can rule out the singlet-singlet energy transfer process. Therefore, the observed quenching could be due to the electron transfer from ^{1}(TPA$_2$-BDP)* to the AlPorF$_3$ unit. The same mechanism could be applied to explain the quenching of the 727 nm band during the 545 nm excitation because 38% of light is absorbed by TPA$_2$-BDP which causes the direct excitation of this moiety.

Upon addition of C$_{60}$-Im to the dyad TPA$_2$-BDP-AlPorF$_3$, the AlPorF$_3$ fluorescence quenches as a result of the formation of the supramolecular triad TPA$_2$-BDP-AlPorF$_3$←Im-C$_{60}$, Figure 2b. Based on the control titrations (TPA$_2$-BDP)-AlPorF$_3$ *vs* Me-Im (Figure S9), AlPorF$_3$-Ph *vs* C$_{60}$-Im (Figure 3) and AlPorF$_3$-Ph *vs* Me-Im (Figure S10) the strong quenching in AlPorF$_3$ fluorescence bands is attributed to the electron transfer from AlPorF$_3$ to C$_{60}$ unit. Additionally, the decrease in AlPorF$_3$ fluorescence (for bands 585 and 643 nm) also suggests that the rate of the electron transfer from TPA$_2$-BDP to ^{1}(AlPorF$_3$)* is similar to or lower than the electron transfer rate from ^{1}(AlPorF$_3$)* to the C$_{60}$ unit.

Spectroelectrochemistry. In order to assist in interpretation of transient spectral data, spectroelectrochemical studies on the porphyrin and chemical oxidation of BDP were performed. Spectral changes during one-electron oxidation and one-

electron reduction processes of $AlPorF_3$ and that of the BDP compounds are shown in Figure S16 and S17. New peaks corresponding to $(AlPorF_3)^{+\bullet}$ were located at 595 and 690 nm while such peaks for $(AlPorF_3)^{-\bullet}$ were located at 568 and 608 nm. The oxidized product of $(BDP)^{+\bullet}$ revealed a new peak at 496 nm while for $(Ph_2\text{-}BDP)^{+\bullet}$ this peak was at 601 nm and for $(TPA_2\text{-}BDP)^{+\bullet}$, two peaks at 528 and 568 nm were observed.

Transient Absorption Spectroscopy. In order to secure evidence of excited state energy and electron transfer events in the dyads and triads, as envisioned from the energy level diagram in Figure 4, systematic femtosecond transient absorption spectral studies were performed. Since, o-DCB is not stable under strong laser irradiation, the transient absorption studies were performed in toluene. The samples were excited at wavelengths corresponding to BDP and $AlPorF_3$ entities. Figure 8a shows the transient absorption spectra of BDP-$AlPorF_3$ dyad at the indicated delay times and at an excitation wavelength of 510 nm corresponding BDP entity of the dyad. Immediately after excitation, a strong negative signal at 508 nm due to ground state bleaching of BDP was observed (see spectrum at 1 ps and Figure S18b for transient spectra of BDP in toluene). Rapid recovery of this peak was associated with

new peaks, viz., positive peaks at 450, 604 and 1230 nm and negative peaks at 550 and 650 nm, respectively due to ground state bleaching and stimulated emission were observed, thus providing direct proof for singlet-singlet energy transfer from $^1BDP^*$ to $AlPorF_3$ in the dyad producing $^1(AlPorF_3)^*$ as energy transfer product (Figure S18a for transient spectra of $AlPorF_3$ in toluene). Kinetic analysis of the transient peaks resulted in an energy transfer rate constant $k_{EnT} = 1.00 \times 10^{10}$ s^{-1}. Figure 8b shows the transient spectra of BDP-$AlPorF_3$ dyad at the excitation wavelength of 550 nm exciting mainly $AlPorF_3$. The instantaneously formed $^1(AlPorF_3)^*$ in the dyad revealed positive peaks at 450, 607 and 1235 nm and negative peaks at 550, 590 and 650 nm. The positive peaks were due to transitions originated from the $^1(AlPorF_3)^*$ state while the negative peaks were due to ground state bleaching and stimulated emission. The right hand panel of Figure 8b shows the decay time profile of the 1235 nm peak of $^1(AlPorF_3)^*$ state for the dyad and the reference $AlPorF_3\text{-}Ph$ compound under similar experimental conditions. The decay profile the dyad largely tracked that of the reference compound, suggesting lack of major photochemical events from the $^1(AlPorF_3)^*$ to covalently linked BDP in the dyad.
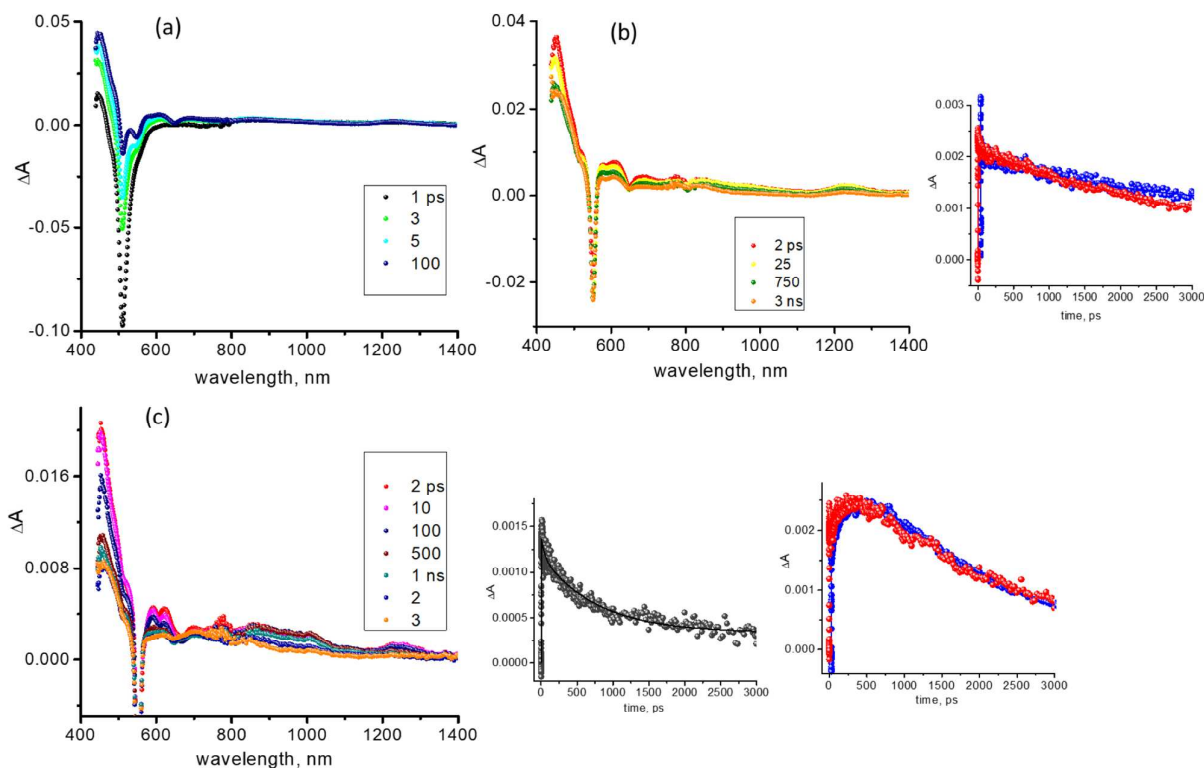
Figure 8. Femtosecond transient absorption spectra at the indicated delay times of (a) BDP-$AlPorF_3$ dyad, excitation wavelength of 510 nm, (b) BDP-$AlPorF_3$ dyad, excitation wavelength of 550 nm (the decay profile of 1235 nm peak corresponding to $^1(AlPorF_3)^*$ for $AlPorF_3$-Ph (red) and BDP-$AlPorF_3$ dyad (blue) is shown on the right), (c) BDP-$AlPorF_3\leftarrow$Im-C_{60} triad, excitation wavelength of 550 nm (decay profile of 1230 nm corresponding to $^1(AlPorF_3)^*$ (black) and 1010 nm of $(C_{60})^{-}$ in the BDP-$AlPorF_3\leftarrow$Im-C_{60} triad (red) and Ph-$AlPorF_3\leftarrow$Im-C_{60} dyad (blue) are shown at the right panel). All spectra were recorded in toluene.

Nanoscale

ARTICLE

The supramolecular triad, BDP-AlPorF$_3$←Im-C$_{60}$ formed by coordinating C$_{60}$-Im to BDP-AlPorF$_3$ revealed excited state charge separation from the ^{1}(AlPorF$_3$)* state as shown in Figure 8c. In the presence of coordinated C$_{60}$-Im, the transient peaks of ^{1}(AlPorF$_3$)* revealed rapid decay/recovery of the positive/negative peaks (see time profile of the 1235 nm peak of ^{1}(AlPorF$_3$)* at the right hand side panel showing rapid decay compared with that shown in the time profiles in Figure 8b) accompanied by new peaks at 690 nm corresponding to (AlPorF$_3$)$^{+\bullet}$ and 1010 nm corresponding to (C$_{60}$)$^{-\bullet}$ species.[63, 68, 69] The time profile of the (C$_{60}$)$^{-\bullet}$ is shown in Figure 8c far right hand panel (red trace); analysis of this kinetic trace resulted in a rate constant for charge separation, k_{CS} of 2.43 x 10^9 s^{-1}. The decay of (C$_{60}$)$^{-\bullet}$ lasted over 3 ns. The time profile of the (C$_{60}$)$^{-\bullet}$ from the reference dyad Ph-AlPorF$_3$←Im-C$_{60}$ (see Figure S19 for femtosecond transient spectra) also shown in Figure 8c far right hand panel (blue trace). The time profiles were almost superimposable (k_{CS} = 2.77 x 10^9 s^{-1} in the case of Ph-AlPorF$_3$←Im-C$_{60}$ dyad). These results suggest that the BDP entity in the BDP-AlPorF$_3$←Im-C$_{60}$ triad is not involved in any electron migration reaction resulting in stabilization of charge separated state, which is consistent with the energy level diagram.

Steady-state fluorescence studies had revealed the occurrence of both energy (42%) and electron (12%) upon excitation of AlPorF$_3$ in the Ph$_2$-BDP-AlPorF$_3$ dyad. The extended conjugation induced red shift of both absorption and fluorescence of Ph$_2$-BDP resulting in switching of energy transfer from ^{1}(AlPorF$_3$)* to ^{1}(Ph$_2$-BDP)* in the case of Ph$_2$-BDP-AlPorF$_3$ dyad compared to ^{1}BDP* to ^{1}(AlPorF$_3$)* observed in the case of BDP-AlPorF$_3$ dyad. Femtosecond transient spectral studies provided evidence for this process as shown in Figure 9a. The spectrum recorded at 1 ps revealed positive peaks at 454, 600, 672 and 1230 nm and negative peaks at 552, 578, 635, and 708 nm. Control experiments performed on pristine Ph$_2$-BDP revealed that the peaks at 578, 630 and 708 nm are indeed due to ^{1}(Ph$_2$-BDP)* (see Figure S18c for transient spectra of Ph$_2$-BDP in toluene). These observations indicate that at a time interval of 1 ps and at the excitation wavelength of 555 nm, ^{1}(Ph$_2$-BDP)* is also formed in addition to ^{1}AlPorF$_3$* due to energy transfer and to some extent by direct excitation. The growth of the 630 nm peak of ^{1}(Ph$_2$-BDP)* continued to develop until about 100 ps, resulting in an energy transfer rate constant, k_{EnT} = 1.00 x 10^{10} s^{-1}. The decay profile of the 1230 nm peak of ^{1}(AlPorF$_3$)* in the dyad (red trace) is compared with that of pristine ^{1}(AlPorF$_3$)* from reference AlPorF$_3$-Ph (blue trace) in Figure 9a right hand panel. Rapid decay in the case of the dyad unequivocally supported photochemical processes originating from ^{1}(AlPorF$_3$)* in the dyad. The charge separated product estimated to be around 12%, was expected to reveal new transient peaks in the 600-610 nm range due to (Ph$_2$-BDP)$^{+\bullet}$-(AlPorF$_3$)$^{-\bullet}$ charge-separated state (see Figures S16 and S17 for spectroelectrochemical results). However, the strong negative peak of ^{1}(Ph$_2$-BDP)* (630 nm) in this wavelength region precluded us from isolating and securing kinetic information of the charge-separated state.

Table 3. Charge separation, hole transfer, and electron migration rates of newly investigated compounds in toluene from *fs*-transient absorption studies.

Compound	Excitation 545 nm	Excitation 500/630/700 nm
Ph-AlPorF$_3$←Im-C$_{60}$	(AlPorF$_3$)$^{+\bullet}$ (C$_{60}$)$^{-\bullet}$: k_{CS} = 2.77 × 10^9 s^{-1}	-
BDP-AlPorF$_3$←Im-C$_{60}$	(AlPorF$_3$)$^{+\bullet}$ (C$_{60}$)$^{-\bullet}$: k_{CS} = 2.43 × 10^9 s^{-1}	^{1}(BDP)*→^{1}(AlPorF$_3$)*: k_{EnT} = 1.00 x 10^{10} s^{-1}
Ph$_2$-BDP-AlPorF$_3$←Im-C$_{60}$	(AlPorF$_3$)$^{+\bullet}$ (C$_{60}$)$^{-\bullet}$: k_{CS} = 3.35 × 10^9 s^{-1} (AlPorF$_3$)$^{+\bullet}$→Ph$_2$-BDP: k_{HS} = 1.00 x 10^9 s^{-1} ^{1}(Ph$_2$-BDP)*→^{1}(AlPorF$_3$)*: k_{EnT} = 1.00 x 10^{10} s^{-1}	-
TPA$_2$-BDP-AlPorF$_3$←Im-C$_{60}$	(TPA$_2$-BDP)$^{+\bullet}$ (AlPorF$_3$)$^{-\bullet}$: k_{CS} = 1.40 x 10^{10} s^{-1} (AlPorF$_3$)$^{-\bullet}$→C$_{60}$: k_{EM} = 4.95 x 10^8 s^{-1}	(TPA$_2$-BDP)$^{+\bullet}$ (AlPorF$_3$)$^{-\bullet}$: k_{CS} = 1.50 x 10^{10} s^{-1} (AlPorF$_3$)$^{-\bullet}$→C$_{60}$: k_{EM} = 7.10 x 10^8 s^{-1}

(estimated error = k±10%).

Nanoscale

ARTICLE
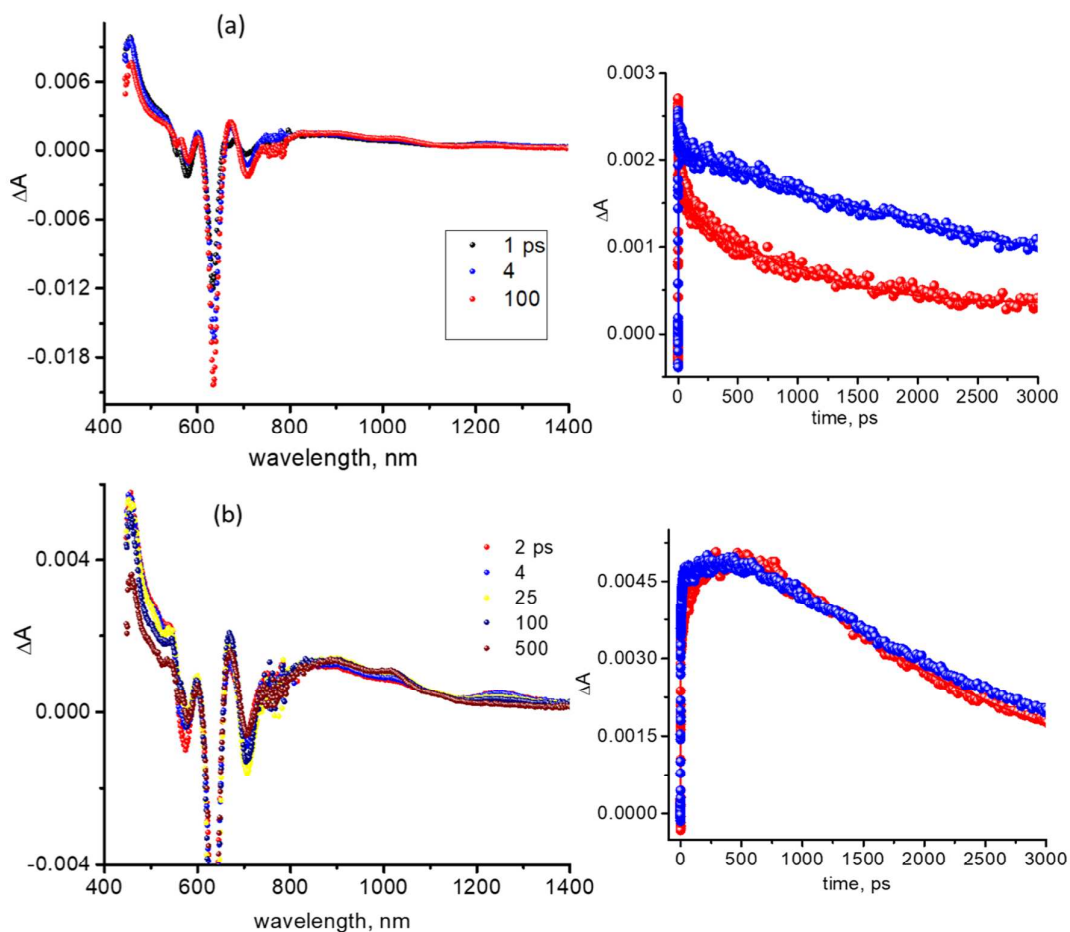
Figure 9. Femtosecond transient absorption spectra at the indicated delay times of (a) Ph$_2$-BDP-AlPorF$_3$ at the excitation wavelength of 555 nm (inset - decay profile of 1230 nm peak corresponding to ^{1}(AlPorF$_3$)* for AlPorF$_3$-Ph (blue) and Ph$_2$-BDP-AlPorF$_3$ (red)), and (b) Ph$_2$-BDP-AlPorF$_3$←Im-C$_{60}$ at 555 nm (inset-decay profile of 1010 nm corresponding to (C$_{60}$)$^{-\bullet}$ in the Ph-AlPorF$_3$←Im-C$_{60}$ dyad (red) and Ph$_2$-BDP-AlPorF$_3$←Im-C$_{60}$ triad (blue)). All spectra were recorded in toluene.

Excited state charge separation was witnessed in the supramolecular triad, Ph$_2$-BDP-AlPorF$_3$←Im-C$_{60}$ as shown in Figure 9b. At the excitation wavelength of 555 nm, the photoexcited species, ^{1}(AlPorF$_3$)* and ^{1}(Ph$_2$-BDP)* revealed faster decay and recovery of the positive and negative peaks, respectively, accompanied by new transient signals corresponding to the formation of charge separated state, distinctively, the (C$_{60}$)$^{-\bullet}$ peak at 1010 nm. The rate of charge separation, k_{ET} was estimated from the growth of (C$_{60}$)$^{-\bullet}$ and was found to be 3.35 x 10^9 s^{-1}, slightly faster than that observed in the case of Ph-AlPorF$_3$←Im-C$_{60}$ being k_{CS} = 2.77 x 10^9 s^{-1}).

The time profile of the (C$_{60}$)$^{-\bullet}$ for the Ph$_2$-BDP-AlPorF$_3$←Im-C$_{60}$ triad (blue) and Ph-AlPorF$_3$←Im-C$_{60}$ dyad (red) are compared in Figure 9b right hand panel. The decay of the (C$_{60}$)$^{-\bullet}$ becomes slower after about 1000 ps in the triad compared to that in the dyad suggesting that the axially coordinated Ph$_2$-BDP is involved in stabilizing the charge separated state by a hole transfer mechanism (see energy level diagram in Figure 4b), that is, by forming (Ph$_2$-BDP)$^{+\bullet}$-AlPorF$_3$←Im-(C$_{60}$)$^{-\bullet}$ charge separated state as the final product. Transient peak of hole transfer product, (Ph$_2$-BDP)$^{+\bullet}$ is expected to occur at 601 nm; although peak growth in this

wavelength region was observed at latter times, the strong negative signal at 630 nm associated with ground state bleaching of $^1AlPorF_3*$ precluded us from further spectral analysis. From the kinetic profile in Figure 9b, estimated hole transfer rate, k_{HS}, from $(AlPorF_3)^{+\bullet}$ to Ph_2-BDP to be about 1.00 x 10^9 s^{-1}. In summary, charge stabilization by an electron transfer/hole transfer mechanism was witnessed in the Ph_2-BDP-AlPorF$_3\leftarrow$Im-C$_{60}$ supramolecular triad.

The transient absorption spectra of TPA$_2$-BDP in toluene is shown in Figure S18d. Positive peaks 468, 553, 750 and 1270 nm due to transitions originating from $^1(TPA_2$-BDP$)*$ and negative peaks at 500, 625 and 697 nm due to the ground state bleaching and stimulated emission were observed. Decay/recovery of the positive/negative peaks were slow, consistent with the fluorescence lifetime of TPA$_2$-BDP being 3.16 ns. Energy level diagram shown in Figure 4c predicted formation of initial $(TPA_2$-BDP$)^{+\bullet}$-$(AlPorF_3)^{-\bullet}$ charge-separated state either from the excitation of TPA$_2$-BDP or AlPorF$_3$ entities. From the earlier discussed spectral studies, a peak at 570 nm for $(TPA_2$-BDP$)^{+\bullet}$, and 568 and 608 nm for $(AlPorF_3)^{-\bullet}$ are expected to show up in the transient spectral measurement supporting the formation of $(TPA_2$-BDP$)^{+\bullet}$-$(AlPorF_3)^{-\bullet}$ charge separated state. The transient absorption spectra of TPA$_2$-BDP-

AlPorF$_3$ in toluene at the excitation wavelengths of 545 nm and 695 nm corresponding to AlPorF$_3$ and TPA$_2$-BDP are shown in Figures 10a and b, respectively. The spectra shown in Figures 10a and b are indeed supportive of charge separation although the initial spectrum obtained at the excitation wavelength of 545 nm (see spectrum recorded at 1 ps) resembled that of $^1(TPA_2$-BDP$)*$ instead of $^1AlPorF_3*$ due to strong overlap of TPA$_2$-BDP absorption in this wavelength region. In both spectra, rapid decay/recovery of the peaks of $^1(TPA_2$-BDP$)*$ was accompanied by new peaks in the 600-610 nm range expected for the charge separated species representing the presence of both radical cation and anion species. The decay profile of the 1280 nm peak of TPA$_2$-BDP, and TPA$_2$-BDP-AlPorF$_3$ dyad is shown in the middle panel. A monoexponential decay fit was satisfactory for the TPA$_2$-BDP while for the TPA$_2$-BDP-AlPorF$_3$ dyad, a biexponential fit was needed at both excitation wavelengths. The short-lived component was ascribed to electron transfer and from the time constants the rate constant for electron transfer, k_{CS} was calculated to be 1.40 x 10^{10} s^{-1} at the excitation wavelength of 545 nm and 1.50 x 10^{10} s^{-1} at the excitation wavelength of 695 nm, respectively, generating the $(TPA_2$-BDP$)^{+\bullet}$-$(AlPorF_3)^{-\bullet}$ charge separated state.
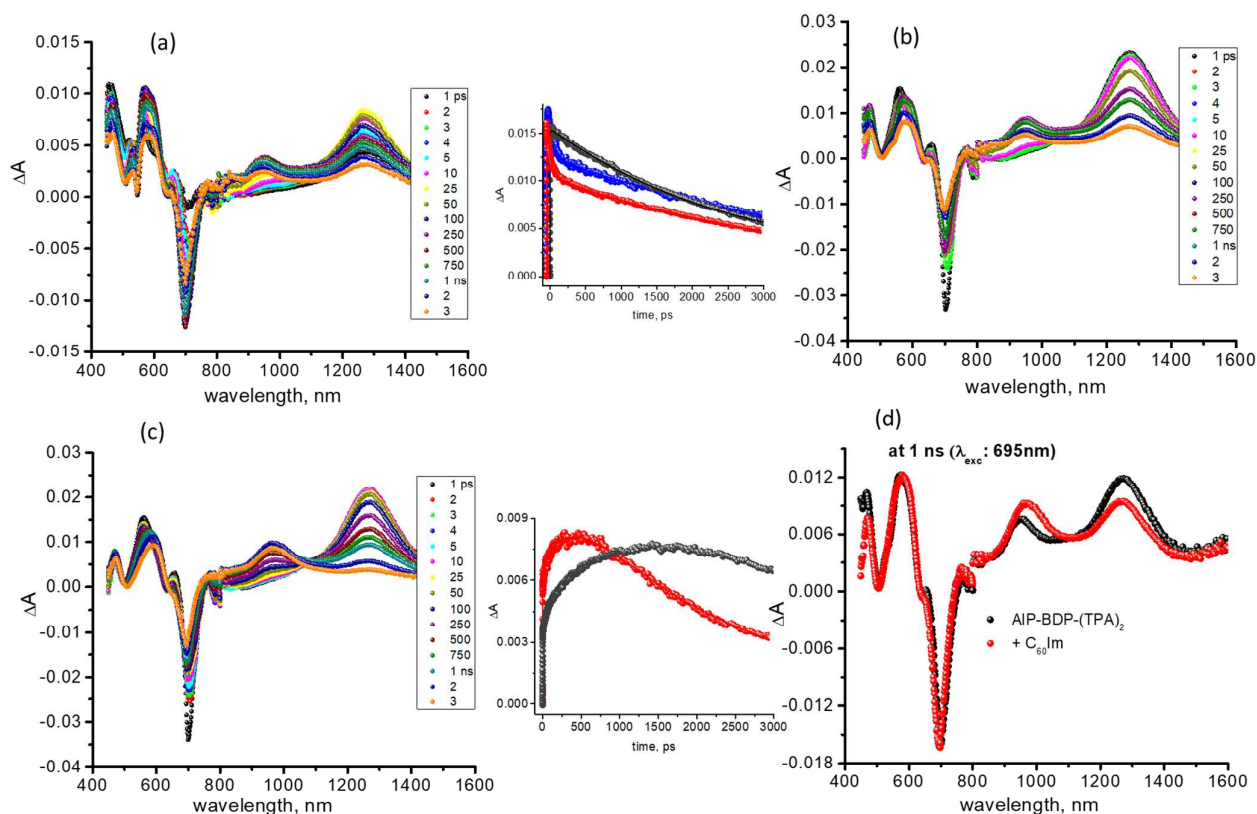
Figure 10. Femtosecond transient absorption spectra at the indicated delay times of (TPA)$_2$-BDP-AlPorF$_3$ dyad at the excitation wavelength of (a) 545 nm and (b) 695 nm. Middle panel - decay profiles of 1280 nm peaks of $^1(TPA_2$-BDP$)*$ for TPA$_2$-BDP (black), dyad at 545 nm excitation (blue) and dyad at 695 nm excitation (red). (c) TPA$_2$-BDP-AlPorF$_3\leftarrow$Im-C$_{60}$ triad at the excitation wavelength of 695 nm. Middle panel – time profile of 1020 nm peak for the triad (black) and Ph-AlPorF$_3\leftarrow$Im-C$_{60}$ dyad (red). (d) transient spectrum at 1 ns delay time of TPA$_2$-BDP-AlPorF$_3$ and TPA$_2$-BDP-AlPorF$_3\leftarrow$Im-C$_{60}$ revealing charge separation. All spectra were recorded in toluene.

Nanoscale

ARTICLE

Transient spectra of the supramolecular TPA$_2$-BDP-AlPorF$_3$←Im-C$_{60}$ triad is shown in Figure 10c. In this system, owing to the facile oxidation of TPA$_2$-BDP compared to AlPorF$_3$, the initial charge separated states, viz., (TPA$_2$-BDP)$^{+\bullet}$-(AlPorF$_3$)$^{-\bullet}$←Im-C$_{60}$ (from TPA$_2$-BDP excitation) and TPA$_2$-BDP-AlPorF$_3^{+}$←Im-(C$_{60}$)$^{-\bullet}$ (from AlPorF$_3$ excitation) could undergo an electron migration in the former case and an hole migration in the latter case to generate (TPA$_2$-BDP)$^{+\bullet}$-AlPorF$_3$←Im-(C$_{60}$)$^{-\bullet}$ as the final charge-separated state. The initial spectra shown in Figure 10c collected by exciting TPA$_2$-BDP (< 5 ps) were supportive of the formation of (TPA$_2$-BDP)$^{+\bullet}$-(AlPorF$_3$)$^{-\bullet}$←Im-C$_{60}$. With time, the 570 nm peak corresponding to (AlPorF$_3$)$^{-\bullet}$ revealed diminished intensity leaving only the 575 nm peak of (TPA)$_2$-BDP$^{\bullet+}$. During this process, the (C$_{60}$)$^{-\bullet}$ peak appeared as a shoulder to the 960 nm peak (see Figure 10d, spectra of the dyad and triad recorded at 1 ns delay time) supporting electron migration from the initial (TPA$_2$-BDP)$^{+\bullet}$-(AlPorF$_3$)$^{-\bullet}$←Im-C$_{60}$ to yield (TPA$_2$-BDP)$^{+\bullet}$-AlPorF$_3$←Im-(C$_{60}$)$^{-\bullet}$. The time profile of (C$_{60}$)$^{-\bullet}$ peak shown in the middle panel shows relatively slow growth of (C$_{60}$)$^{-\bullet}$ compared to that shown in Figure 9b for Ph-AlPorF$_3$←Im-C$_{60}$, supporting its formation from the secondary electron migration step. From the kinetic profile, the estimated rate of electron migration, k_{EM} was found to be 7.1 x 10^8 s^{-1}. Similar results were also observed when the sample was excited at 545 nm (exciting both TPA$_2$-BDP and AlPorF$_3$ entities. The hole transfer rate (k_{HS}) estimated from monitoring the time profile of 960 nm peak was found to be 4.95 x 10^8 s^{-1}. In case of both TPA$_2$-BDP-AlPorF$_3$ dyad and TPA$_2$-BDP-AlPorF$_3$←Im-C$_{60}$ triad a slow decaying new peak in the 960 nm range was observed at latter times and was tentatively assigned to ^{3}(TPA$_2$-BDP)*, likely formed during the process of charge recombination. To summarize, in the case of TPA$_2$-BDP-AlPorF$_3$←Im-C$_{60}$ triad, distantly separated radical ion-pair was possible to establish.

In both Ph$_2$-BDP-AlPorF$_3$←Im-C$_{60}$ and TPA$_2$-BDP-AlPorF$_3$←Im-C$_{60}$ triads, the decay of the (C$_{60}$)$^{-\bullet}$ lasted over 3 ns, the monitoring time window of our instrument. Thus, nanosecond transient spectra were recorded under similar experimental conditions. However, in both systems, a signal representing the existence of (C$_{60}$)$^{-\bullet}$ was rather weak even at the earliest detection limit of 20 ns. Thus, it is safe to conclude that the radical ion-pairs in these triads persists for about 20 ns.

Photoinduced processes in triads. The rich redox and optical properties of the selected AlPorF$_3$ and BDP entities, allow us to demonstrate excitation wavelength dependent photochemical events in the investigated triads. In BDP-AlPorF$_3$←Im-C$_{60}$ triad system, excitation of AlPorF$_3$ moiety results electron transfer from ^{1}(AlPorF$_3$)* to C$_{60}$ to form the radical pair BDP-(AlPorF$_3$)$^{+\bullet}$←Im-(C$_{60}$)$^{-\bullet}$. In contrary, excitation of BDP moiety induces rapid energy transfer from ^{1}BDP* to ^{1}(AlPorF$_3$)*. Hence, BDP entity could be used as a light-harvesting antenna in this system. In the case of triad, Ph$_2$-BDP-AlPorF$_3$←Im-C$_{60}$, excitation of AlPorF$_3$ causes charge separation followed by hole shift to produce a final radical pair, viz., Ph$_2$-BDP-^{1}(AlPorF$_3$)*←Im-C$_{60}$ ⇒ Ph$_2$-BDP-(AlPorF$_3$)$^{+\bullet}$←Im-(C$_{60}$)$^{-\bullet}$ ⇒ (Ph$_2$-BDP)$^{+\bullet}$-AlPorF$_3$←Im-(C$_{60}$)$^{-\bullet}$. However, this sequential electron transfer seems to be exist as a minor component as most of the excited state, ^{1}(AlPorF$_3$)*, is quenched by energy transfer to ^{1}(Ph$_2$-BDP)*. Moreover, this competing energy transfer process is one order magnitude faster than the charge separation and hole shift processes, see Table 3. On the other hand, no major photochemical events upon excitation of Ph$_2$-BDP in the triad was witnessed. Finally, in the case of triad, TPA$_2$-BDP-AlPorF$_3$←Im-C$_{60}$, excitation of AlPorF$_3$ or TPA$_2$-BDP both results a same final radical pair, however, they are produced via two different routes, **route 1**: TPA$_2$-BDP-^{1}(AlPorF$_3$)*←Im-C$_{60}$ ⇒ TPA$_2$-BDP-(AlPorF$_3$)$^{+\bullet}$←Im-(C$_{60}$)$^{-\bullet}$ ⇒ (TPA$_2$-BDP)$^{+\bullet}$-AlPorF$_3$←Im-(C$_{60}$)$^{-\bullet}$ and **route 2**: TPA$_2$-BDP-^{1}(AlPorF$_3$)*←Im-C$_{60}$ ⇒ (TPA$_2$-BDP)$^{+\bullet}$-(AlPorF$_3$)$^{-\bullet}$←Im-C$_{60}$⇒ (TPA$_2$-BDP)$^{+\bullet}$-AlPorF$_3$←Im-(C$_{60}$)$^{-\bullet}$. The fact that the charge separation between TPA$_2$-BDP and AlPorF$_3$ in the triad is one order magnitude faster than the charge separation between AlPorF$_3$ and C$_{60}$ (see Table 3), it is more likely that the route 2 is major process in this system. Moreover, such fast charge separation could out-compete the energy transfer process from ^{1}(AlPorF$_3$)* to ^{1}(TPA$_2$-BDP)*.

Conclusions

The results presented above show the successful mimicking of the broad band capturing axially linked artificial photosynthetic reaction centers by exploiting the unique properties of AlPorF$_3$, BDP derivative and C$_{60}$ entities. Ground state properties suggest that the triad components are spatially well separated without any electronic interactions. The photoinduced processes were established by using the steady-state fluorescence and femtosecond transient absorbance studies. The TPA$_2$-BDP derivatives are equipped with better potentials than the Ph$_2$-BDP and BDP derivatives for sequential electron transfer in investigated triads. Also, the extended conjugate structure of TPA$_2$-BDP provided the panchromatic effect. The present studies showed that the inclusion of styryl groups in the triad structure certainly improved the optical sensitivity but its extended structure exhibited a modest influence in stabilization of the final radical pair, (BDP derivative)$^{+\bullet}$-(C$_{60}$)$^{-\bullet}$. Currently,

studies are in progress to improve the stabilization of radical pairs.

Conflicts of interest

There are no conflicts to declare.

Acknowledgements

References

1. J. Barber and B. Andersson, *Nature*, 1994, **370**, 31-34.
2. J. Deisenhofer, Norris, J. R., ed., *The Photosynthetic Reaction Center*, Academic Press, San Diego, CA, 1993.
3. J. Deisenhofer, O. Epp, K. Miki, R. Huber and H. Michel, *J. Mol. Biol.*, 1984, **180**, 385-398.
4. P. Fromme, *Curr. Opin. Struct. Biol.*, 1996, **6**, 473-484.
5. F. D'Souza and O. Ito, *Coord. Chem. Rev.*, 2005, **249**, 1410-1422.
6. F. D'Souza, P. M. Smith, M. E. Zandler, A. L. McCarty, M. Itou, Y. Araki and O. Ito, *J. Am. Chem. Soc.*, 2004, **126**, 7898-7907.
7. S. Fukuzumi, *Phys. Chem. Chem. Phys.*, 2008, **10**, 2283-2297.
8. D. M. Guldi, *Chem. Soc. Rev.*, 2002, **31**, 22-36.
9. D. Gust and T. A. Moore, *Top. Curr. Chem.*, 1991, **159**, 103-151.
10. D. Gust, T. A. Moore and A. L. Moore, *Acc. Chem. Res.*, 2001, **34**, 40-48.
11. H. Imahori, Y. Mori and Y. Matano, *J. Photochem. Photobiol. C-Photochem. Rev.*, 2003, **4**, 51-83.
12. P. V. Kamat, *J. Phys. Chem. C*, 2007, **111**, 2834-2860.
13. G. Kodis, Y. Terazono, P. A. Liddell, J. Andreasson, V. Garg, M. Hambourger, T. A. Moore, A. L. Moore and D. Gust, *J. Am. Chem. Soc.*, 2006, **128**, 1818-1827.
14. C. Luo, D. M. Guldi, H. Imahori, K. Tamaki and K. Sakata, *J. Am. Chem. Soc.*, 2000, **122**, 6535-6551.
15. M. R. Wasielewski, *J. Org. Chem.*, 2006, **71**, 5051-5066.
16. M. R. Wasielewski, *Acc. Chem. Res.*, 2009, **42**, 1910-1921.
17. M. E. El-Khoulya, E. El-Mohsnawy and S. Fukuzumi, *J. Photochem. Photobiol. C-Photochem. Rev.*, 2017, **31**, 36-83.
18. D. Gust, in *Artificial Photosynthesis*, ed. R. Bruno, Academic Press Ltd-Elsevier Science Ltd, London, 2016, vol. 79, pp. 1-42.
19. S. Fukuzumi, K. Ohkubo and T. Suenobu, *Acc. Chem. Res.*, 2014, **47**, 1455-1464.
20. P. D. W. Boyd and C. A. Reed, *Acc. Chem. Res.*, 2005, **38**, 235-242.
21. D. Curiel, K. Ohkubo, J. R. Reimers, S. Fukuzumi and M. J. Crossley, *Phys. Chem. Chem. Phys.*, 2007, **9**, 5260-5266.
22. F. D'Souza, S. Gadde, D. M. S. Islam, C. A. Wijesinghe, A. L. Schumacher, M. E. Zandler, Y. Araki and O. Ito, *J. Phys. Chem. A*, 2007, **111**, 8552-8560.
23. M. Di Valentin, A. Bisol, G. Agostini, P. A. Liddell, G. Kodis, A. L. Moore, T. A. Moore, D. Gust and D. Carbonera, *J. Phys. Chem. B*, 2005, **109**, 14401-14409.
24. S. L. Gould, G. Kodis, R. E. Palacios, L. de la Garza, A. Brune, D. Gust, T. A. Moore and A. L. Moore, *J. Phys. Chem. B*, 2004, **108**, 10566-10580.
25. A. Harriman and J. P. Sauvage, *Chem. Soc. Rev.*, 1996, **25**, 41-&.
26. J. Y. Liu, M. E. El-Khouly, S. Fukuzumi and D. K. P. Ng, *Chem.-Eur. J.*, 2011, **17**, 1605-1613.
27. K. M. S. a. R. G. K. M. Kadish, ed., *Handbook of Porphyrin Science*, World Scientific, Singapore, 2010.
28. P. K. Poddutoori, P. Poddutoori, B. G. Maiya, T. K. Prasad, Y. E. Kandrashkin, S. Vasil'ev, D. Bruce and A. van der Est, *Inorg. Chem.*, 2008, **47**, 7512-7522.
29. H. Imahori, D. M. Guldi, K. Tamaki, Y. Yoshida, C. P. Luo, Y. Sakata and S. Fukuzumi, *J. Am. Chem. Soc.*, 2001, **123**, 6617-6628.
30. C. B. Kc, G. N. Lim and F. D'Souza, *Nanoscale*, 2015, **7**, 6813-6826.
31. H. Imahori, *Org. Biomol. Chem.*, 2004, **2**, 1425-1433.
32. H. Imahori, *J. Phys. Chem. B*, 2004, **108**, 6130-6143.
33. H. Imahori, K. Hagiwara, T. Akiyama, M. Aoki, S. Taniguchi, T. Okada, M. Shirakawa and Y. Sakata, *Chem. Phys. Lett.*, 1996, **263**, 545-550.
34. H. Imahori, K. Tamaki, D. M. Guldi, C. P. Luo, M. Fujitsuka, O. Ito, Y. Sakata and S. Fukuzumi, *J. Am. Chem. Soc.*, 2001, **123**, 2607-2617.
35. P. A. Liddell, G. Kodis, L. de la Garza, J. L. Bahr, A. L. Moore, T. A. Moore and D. Gust, *Helv. Chim. Acta*, 2001, **84**, 2765-2783.
36. P. A. Liddell, G. Kodis, L. de la Garza, A. L. Moore, T. A. Moore and D. Gust, *J. Phys. Chem. B*, 2004, **108**, 10256-10265.
37. A. L. M. Haffa, S. Lin, J. C. Williams, B. P. Bowen, A. K. W. Taguchi, J. P. Allen and N. W. Woodbury, *J. Phys. Chem. B*, 2004, **108**, 4-7.
38. A. Bagaki, H. B. Gobeze, G. Charalambidis, A. Charisiadis, C. Stangel, V. Nikolaou, A. Stergiou, N. Tagmatarchis, F. D'Souza and A. G. Coutsolelos, *Inorg. Chem.*, 2017, **56**, 10268-10280.
39. P. K. Poddutoori, L. P. Bregles, G. N. Lim, P. Boland, R. G. Kerr and F. D'Souza, *Inorg. Chem.*, 2015, **54**, 8482-8494.
40. P. K. Poddutoori, G. N. Lim, A. S. D. Sandanayaka, P. A. Karr, O. Ito, F. D'Souza, M. Pilkington and A. van der Est, *Nanoscale*, 2015, **7**, 12151-12165.
41. P. K. Poddutoori, G. N. Lim, S. Vassiliev and F. D'Souza, *Phys. Chem. Chem. Phys.*, 2015, **17**, 26346-26358.
42. P. K. Poddutoori, A. S. D. Sandanayaka, T. Hasobe, O. Ito and A. van der Est, *J. Phys. Chem. B*, 2010, **114**, 14348-14357.
43. P. K. Poddutoori, A. S. D. Sandanayaka, N. Zarrabi, T. Hasobe, O. Ito and A. van der Est, *J. Phys. Chem. A*, 2011, **115**, 709-717.
44. P. K. Poddutoori, N. Zarrabi, A. G. Moiseev, R. Gumbau-Brisa, S. Vassiliev and A. van der Est, *Chem.-Eur. J.*, 2013, **19**, 3148-3161.
45. V. Bandi, M. E. El-Khouly, V. N. Nesterov, P. A. Karr, S. Fukuzumi and F. D'Souza, *J. Phys. Chem. C*, 2013, **117**, 5638-5649.
46. V. Bandi, H. B. Gobeze, P. A. Karr and F. D'Souza, *J. Phys. Chem. C*, 2014, **118**, 18969-18982.

47. V. Bandi, K. Ohkubo, S. Fukuzumi and F. D'Souza, *Chem. Commun.*, 2013, **49**, 2867-2869.
48. G. A. Metselaar, J. K. M. Sanders and J. de Mendoza, *Dalton Trans.*, 2008, DOI: 10.1039/b717017n, 588-590.
49. A. Amati, P. Cavigli, A. Kahnt, M. T. Indelli and E. Iengo, *J. Phys. Chem. A*, 2017, **121**, 4242-4252.
50. G. J. E. Davidson, L. H. Tong, P. R. Raithby and J. K. M. Sanders, *Chem. Commun.*, 2006, DOI: 10.1039/b605435h, 3087-3089.
51. E. Iengo, G. D. Pantos, J. K. M. Sanders, M. Orlandi, C. Chiorboli, S. Fracasso and F. Scandola, *Chem. Sci.*, 2011, **2**, 676-685.
52. E. Iengo, P. Cavigli, M. Gamberoni and M. T. Indelli, *Eur. J. Inorg. Chem.*, 2014, **2014**, 337-344.
53. E. Maligaspe, N. V. Tkachenko, N. K. Subbaiyan, R. Chitta, M. E. Zandler, H. Lemmetyinen and F. D'Souza, *J. Phys. Chem. A*, 2009, **113**, 8478-8489.
54. X. F. Chen, M. E. El-Khouly, K. Ohkubo, S. Fukuzumi and D. K. P. Ng, *Chem.-Eur. J.*, 2018, **24**, 3862-3872.
55. G. N. Lim, E. Maligaspe, M. E. Zandler and F. D'Souza, *Chem.-Eur. J.*, 2014, **20**, 17089-17099.
56. C. B. Kc, G. N. Lim, V. N. Nesterov, P. A. Karr and F. D'Souza, *Chem.-Eur. J.*, 2014, **20**, 17100-17112.
57. M. E. El-Khouly, S. Fukuzumi and F. D'Souza, *ChemPhysChem*, 2014, **15**, 30-47.
58. C. O. Obondi, G. N. Lim, P. A. Karr, V. N. Nesterov and F. D'Souza, *Phys. Chem. Chem. Phys.*, 2016, **18**, 18187-18200.
59. M. Fujutsuka and O. Ito, in *Handbook of Photochemistry and Photobiology*, ed. H. S. Nalwa, 2003, vol. 2 Organic Photochemistry, pp. 111-145.
60. D. Guldi and N. Martin, eds., *Electron Transfer in Functionalized Fullerenes. In Fullerenes: From Synthesis to Optoelectronic Properties* Kluwer Academic Publishers, Norwell, MA, 2002.
61. D. M. Guldi, *Chem. Commun.*, 2000, 321-327.
62. H. S. Nalwa, ed., *Photochemistry of Fullernes. In Handbook of Photochemistry and Photobiology, vol. 2; Organic Photochemistry*, 2003.
63. G. N. Lim, S. Hedstrom, K. A. Jung, P. A. D. Smith, V. S. Batista, F. D'Souza, A. van der Est and P. K. Poddutoori, *J. Phys. Chem. C*, 2017, **121**, 14484-14497.
64. H. A. Benesi and J. H. Hildebrand, *J. Am. Chem. Soc.*, 1949, **71**, 2703-2707.
65. D. Rehm and A. Weller, *Ber. Bunsen Ges. Phys. Chem.*, 1969, **73**, 834-839.
66. D. Rehm and A. Weller, *Isr. J. Chem.*, 1970, **8**, 259-&.
67. A. Weller, *Z. Phys. Chem.*, 1982, **133**, 93-98.
68. T. Kato, T. Kodama, T. Shida, T. Nakagawa, Y. Matsui, S. Suzuki, H. Shiromaru, K. Yamauchi and Y. Achiba, *Chem. Phys. Lett.*, 1991, **180**, 446-450.
69. R. J. Sension, C. M. Phillips, A. Z. Szarka, W. J. Romanow, A. R. McGhie, J. P. McCauley, A. B. Smith and R. M. Hochstrasser, *J. Phys. Chem.*, 1991, **95**, 6075-6078.

Graphical Abstract:

Charge-Separation in Panchromatic, Vertically Positioned Bis(donorstyryl)BODIPY – Aluminum(III) Porphyrin – Fullerene Supramolecular Triads

Niloofar Zarrabi, Christopher O. Obondi, Gary N. Lim, Sairaman Seetharaman, Benjamin G. Boe, Francis D'Souza, Prashanth K. Poddutoori

Three, broad band capturing, vertically aligned supramolecular triads, R_2-BODIPY-AlPorF$_3$←Im-C$_{60}$ (R = H, styryl, and C_2H_2-TPA; ← = coordinate bond), have been constructed using axial-bonding capability of aluminum(III) porphyrin. Photoexcitation of the triad results in charge separation followed by rapid hole shift or electron migration to produce $(R_2$-BDP$)^{+\bullet}$-AlPorF$_3$←Im-$(C_{60})^{-\bullet}$ as a final radical pair. The results reveal successful charge stabilization and the charge-separated state persist about 20 ns in these self-assembled supramolecular reaction center mimics.